Supporting Information

September 5, 2016

Toward a Modular Multi-material Nanoparticle Synthesis and Assembly Strategy via Bionanocombinatorics: Bifunctional Peptides for Linking Au and Ag Materials

Beverly D. Briggs,[1,‡,•] J. Pablo Palafox-Hernandez,[2,‡] Yue Li,[3] Chang-Keun Lim,[4] Taylor J. Woehl,[5] Nicholas M. Bedford,[5] Soenke Seifert,[6] Mark T. Swihart,[3,*] Paras N. Prasad,[4] Tiffany R. Walsh,[2,*] Marc R. Knecht[1,*]

1. Department of Chemistry, University of Miami, 1301 Memorial Drive, Coral Gables, Florida 33146, United States

2. Institute for Frontier Materials, Deakin University, Geelong, Victoria 3216, Australia

3. Department of Chemical and Biological Engineering, University at Buffalo (SUNY), Buffalo, New York 14260, United States

4. Department of Chemistry and Institute for Lasers, Photonics, and Biophotonics, University at Buffalo (SUNY), Buffalo, New York 14260, United States

5. Applied Chemicals and Materials Division, National Institute of Standards and Technology, Boulder, Colorado 80305, United States.

6. X-ray Science Division, Argonne National Laboratory, 9700 South Cass Avenue, Argonne, Illinois 60439, United States

(51 pages)

Table S1. Sizing data for Ag and Au capped PARE nanoparticles.

	1:1	2:1	3:1	4:1
trans PARE Ag	11.8 ± 4.6 nm	10.9 ± 3.6 nm	10.9 ± 4.7 nm	11.5 ± 4.2 nm
cis PARE Ag	24.0 ± 6.9 nm	30.8 ± 10.5 nm	17.4 ± 4.4 nm	16.4 ± 6.5 nm
trans PARE Au	1.8 ± 0.4 nm	2.0 ± 0.4 nm	2.6 ± 0.5 nm	4.4 ± 0.8 nm 8.2 ± 1.1 nm
cis PARE Au	2.3 ± 0.5 nm	2.9 ± 0.7 nm	2.7 ± 0.6 nm	4.8 ± 1.3 nm 12.0 ± 2.9 nm

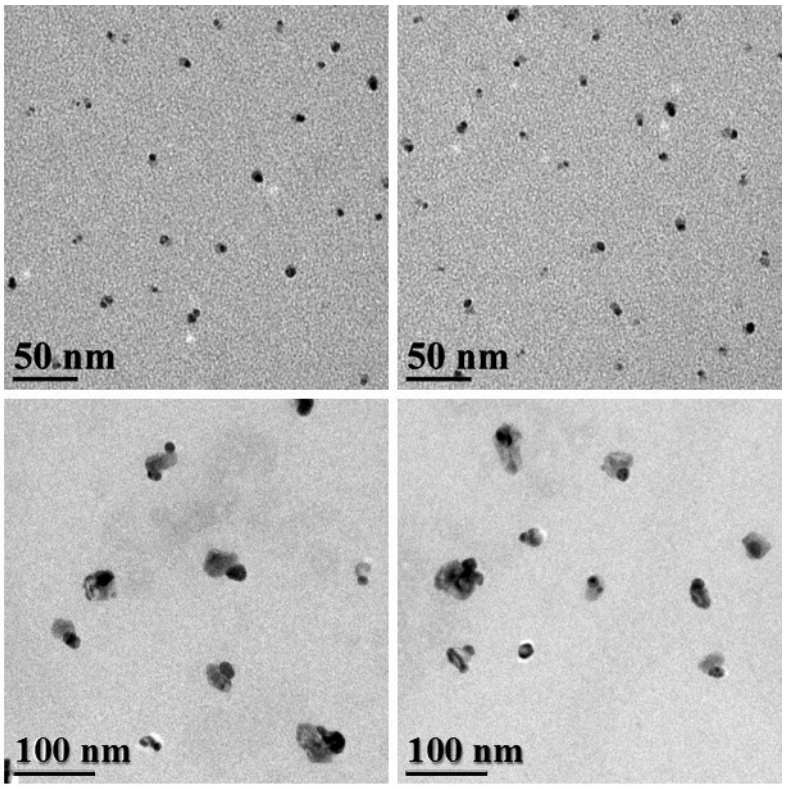

Figure S1. Additional TEM images of 1:1 Ag:*trans* PARE.

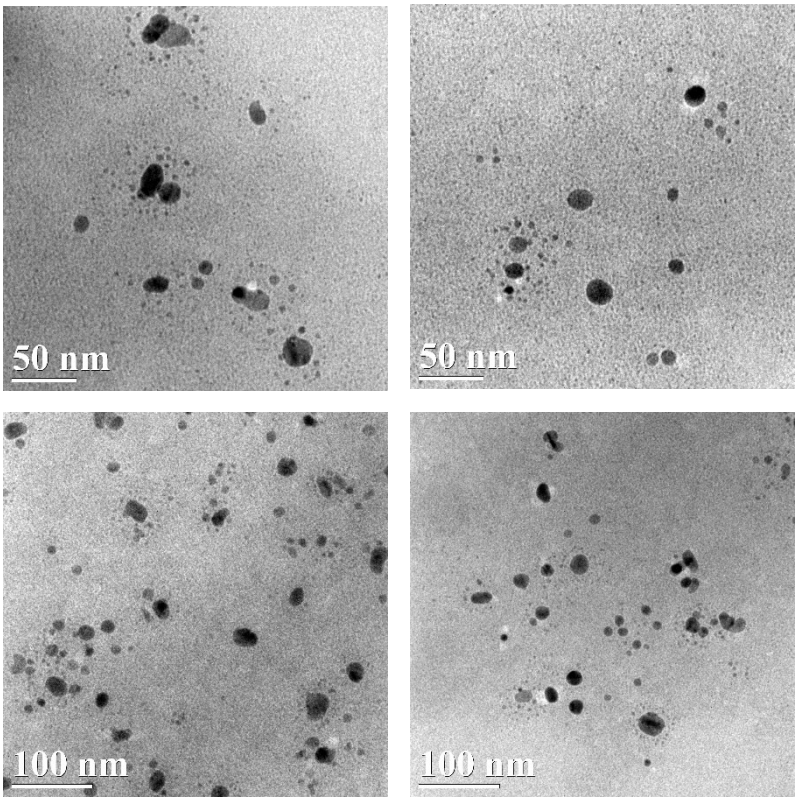

Figure S2. Additional TEM images of 2:1 Ag:*trans* PARE.

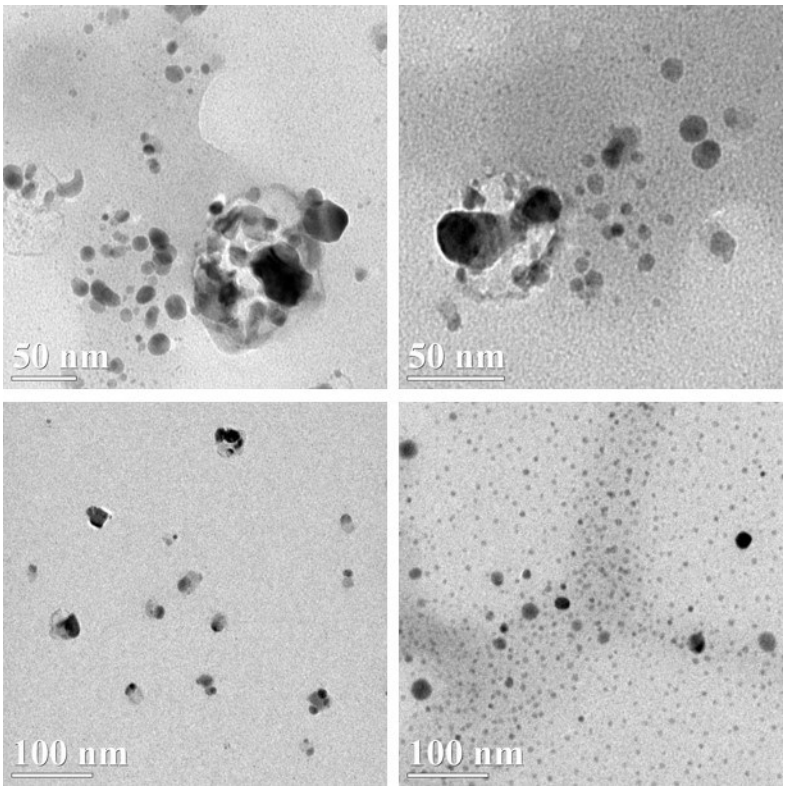

Figure S3. Additional TEM images of 3:1 Ag:*trans* PARE.

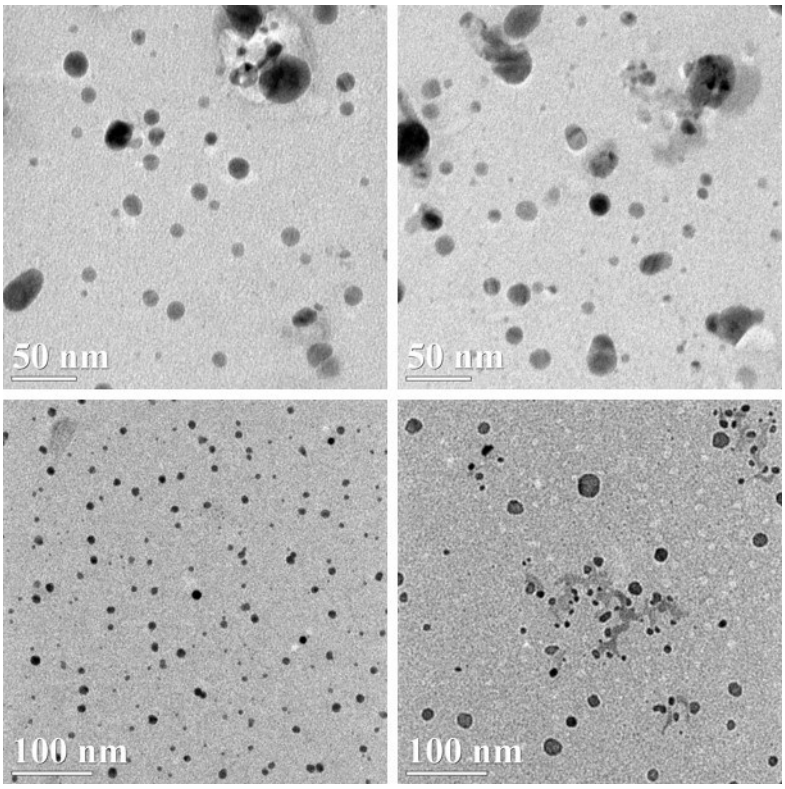

Figure S4. Additional TEM images of 4:1 Ag:*trans* PARE.

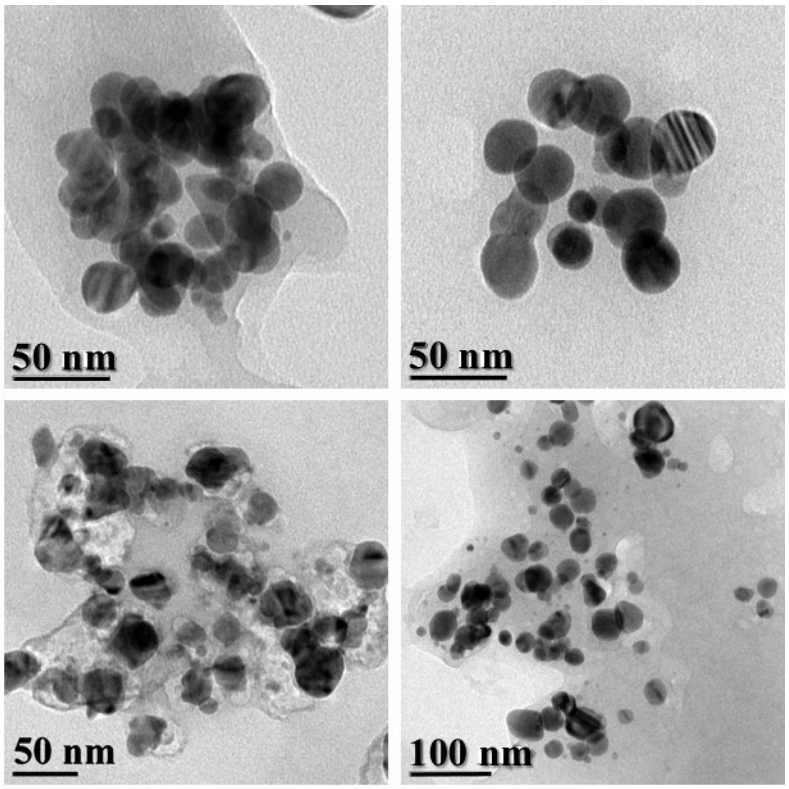

Figure S5. Additional TEM images of 1:1 Ag:*cis* PARE.

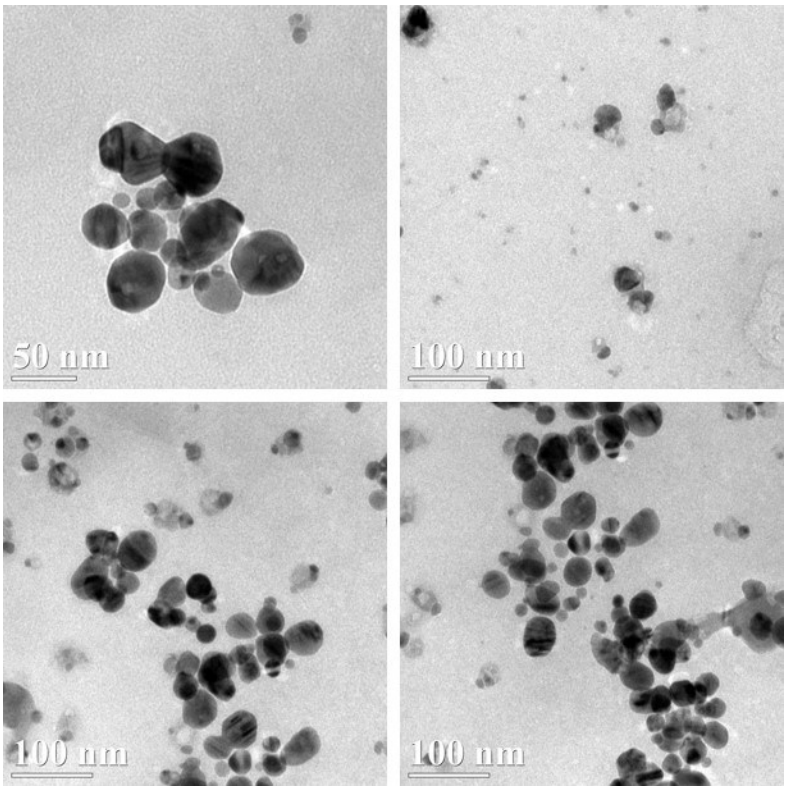

Figure S6. Additional TEM images of 2:1 Ag:*cis* PARE.

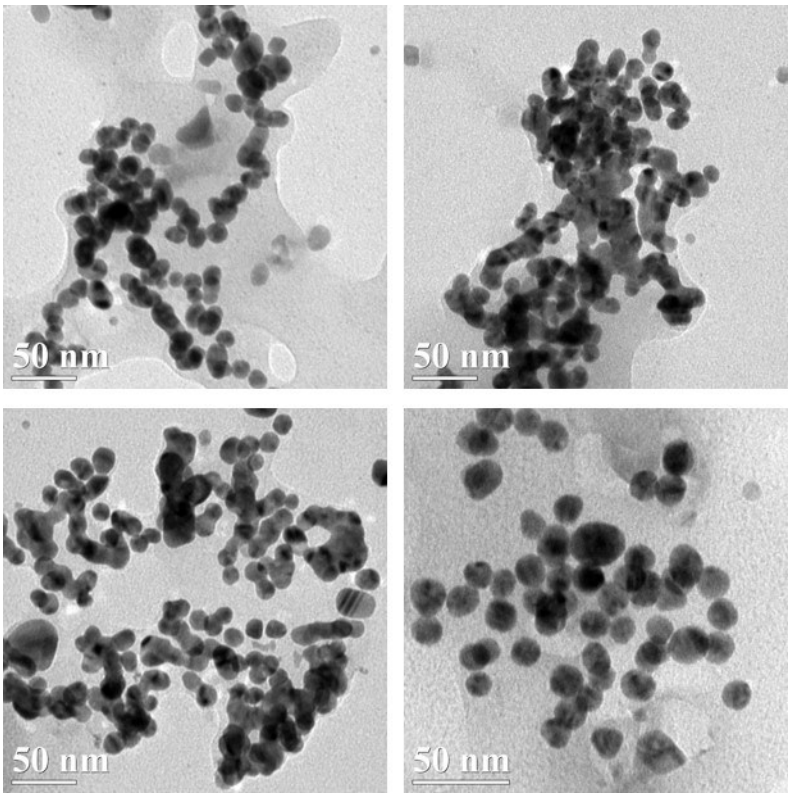

Figure S7. Additional TEM images of 3:1 Ag:*cis* PARE.

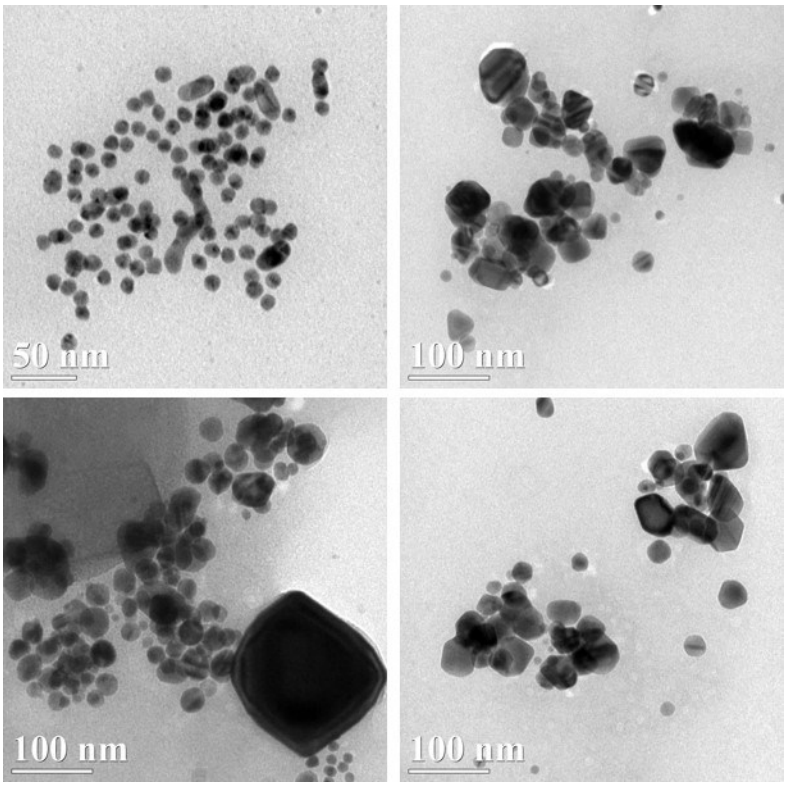

Figure S8. Additional TEM images of 4:1 Ag:*cis* PARE.

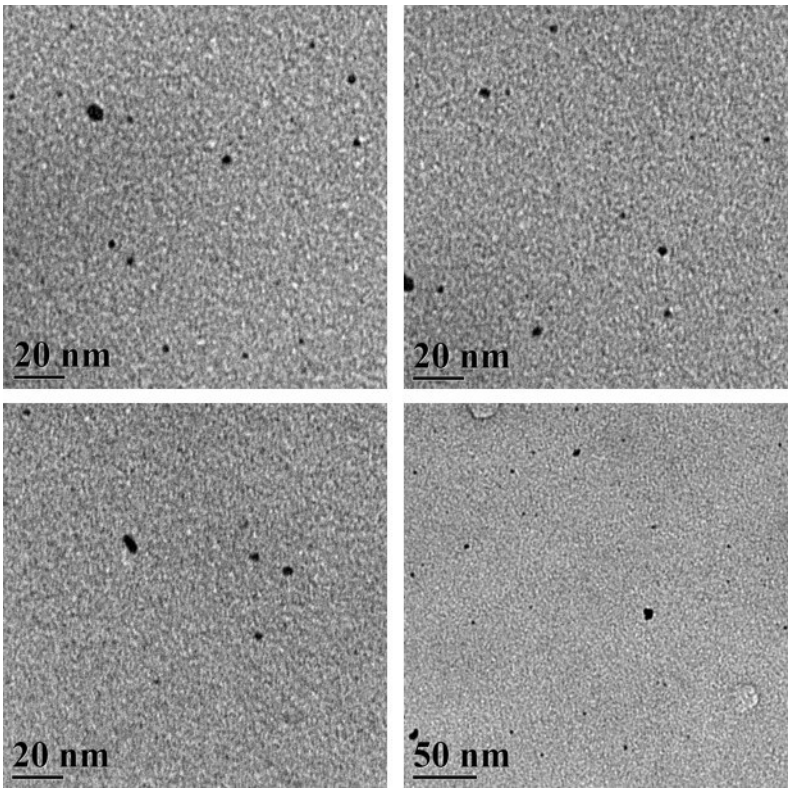

Figure S9. Additional TEM images of 1:1 Au:*trans* PARE.

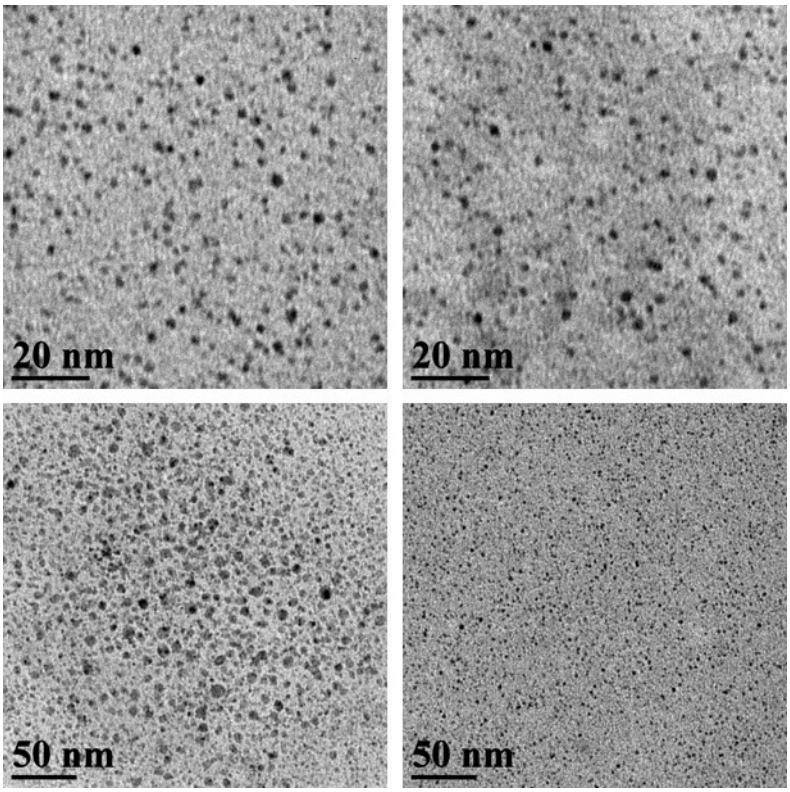

Figure S10. Additional TEM images of 2:1 Au:*trans* PARE.

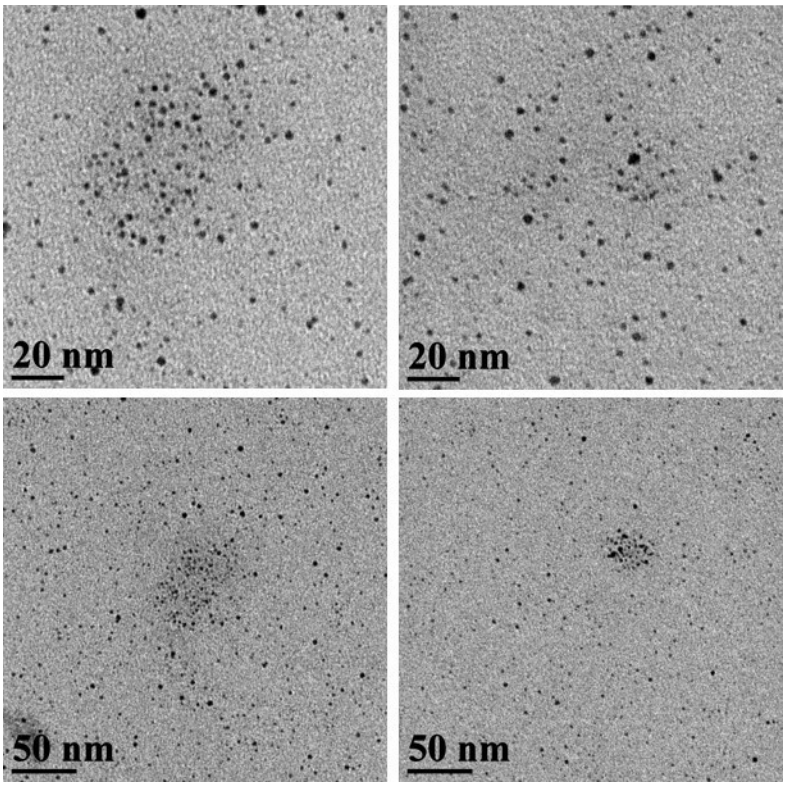

Figure S11. Additional TEM images of 3:1 Au:*trans* PARE.

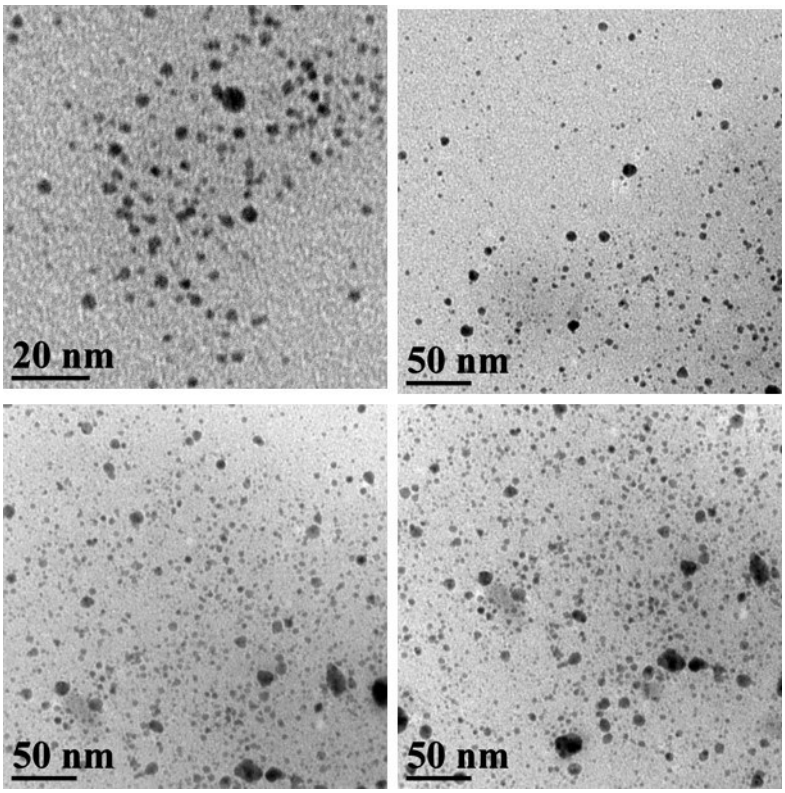

Figure S12. Additional TEM images of 4:1 Au:*trans* PARE.

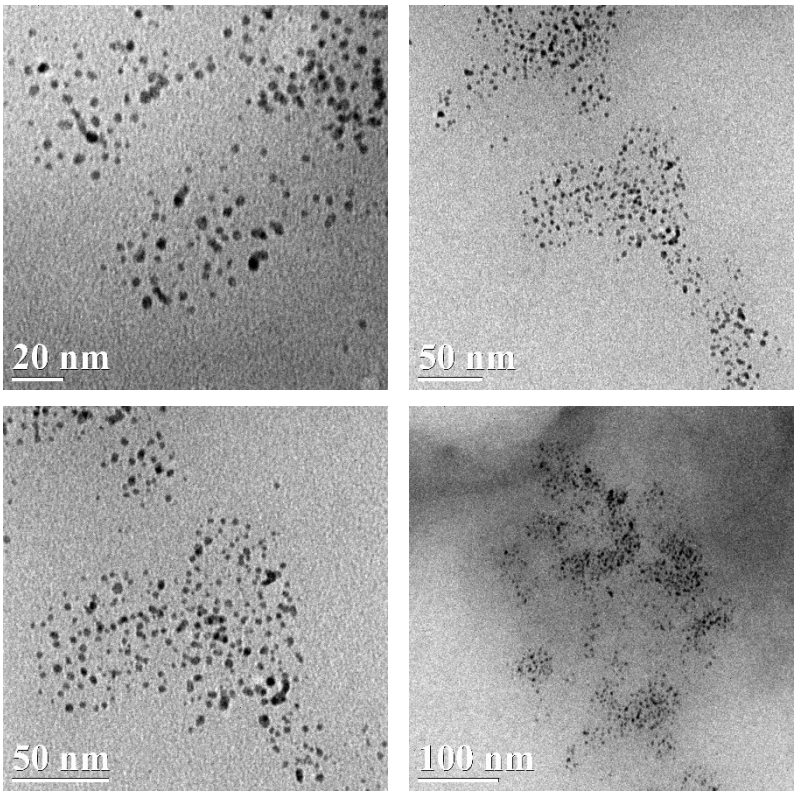

Figure S13. Additional TEM images of 1:1 Au:*cis* PARE.

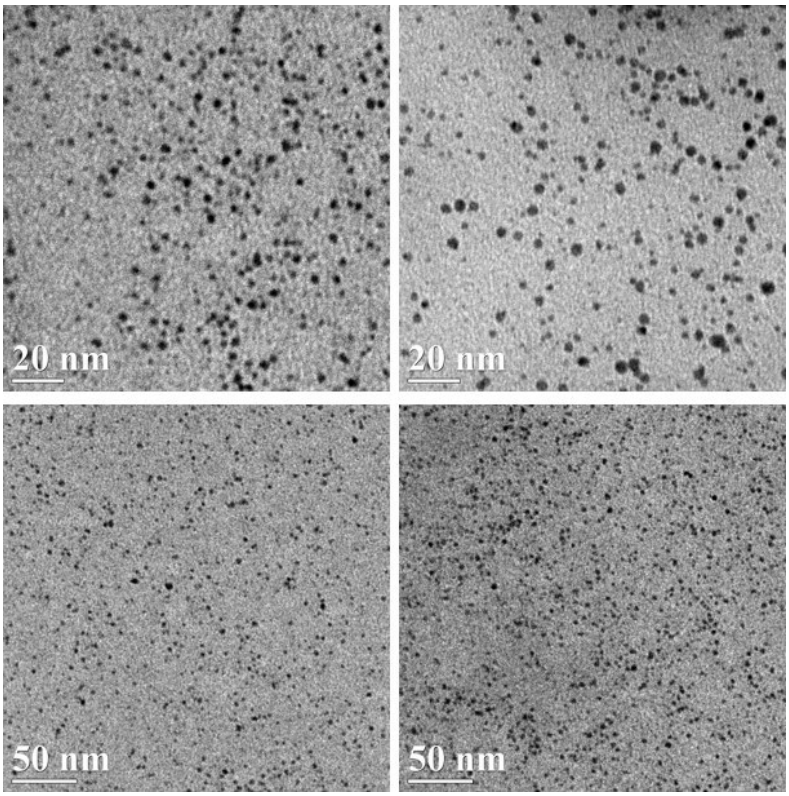

Figure S14. Additional TEM images of 2:1 Au:*cis* PARE.

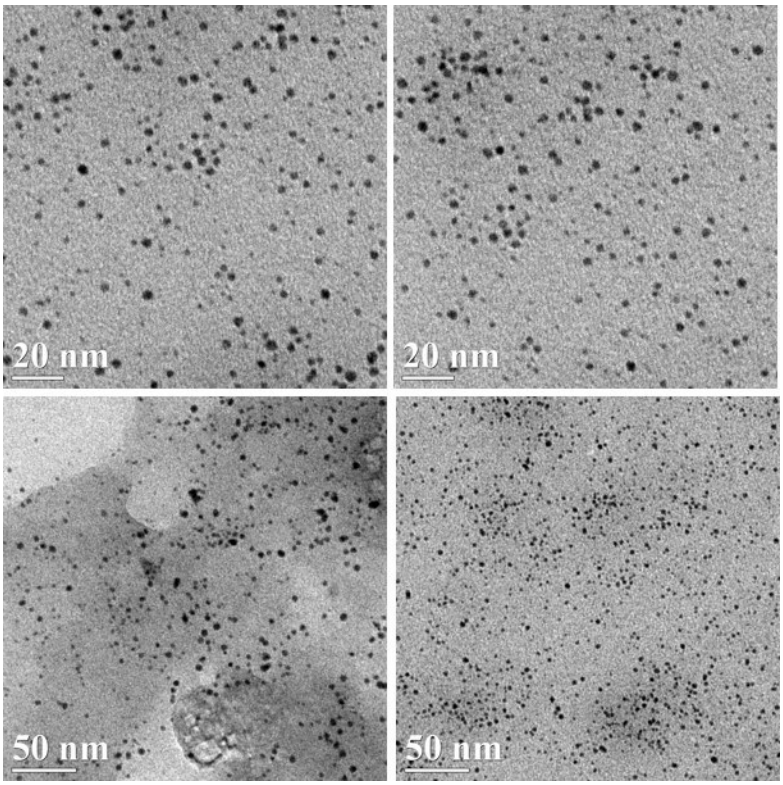

Figure S15. Additional TEM images of 3:1 Au:*cis* PARE.

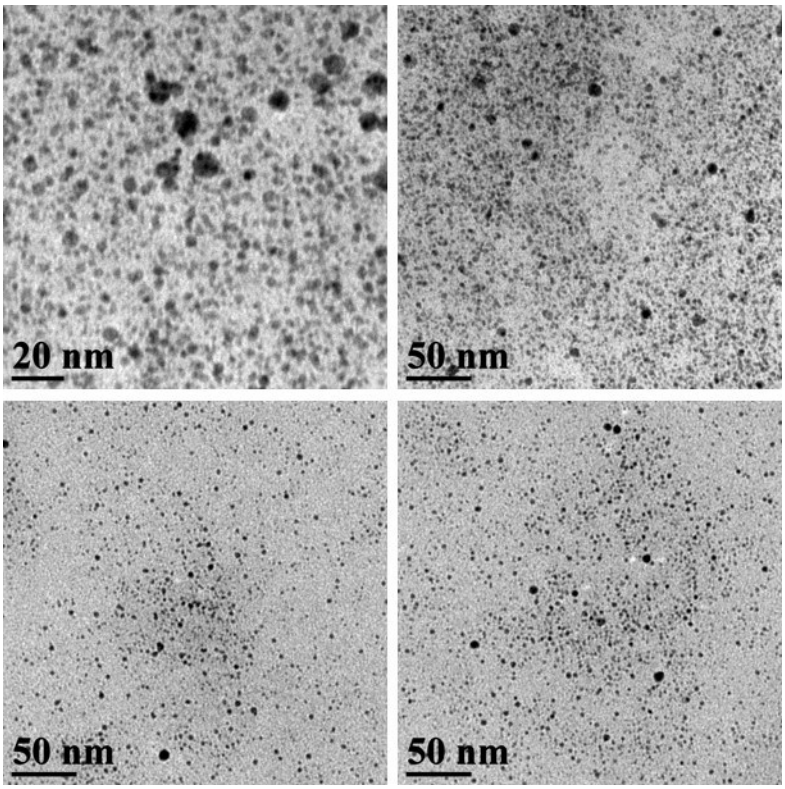

Figure S16. Additional TEM images of 4:1 Au:*cis* PARE.

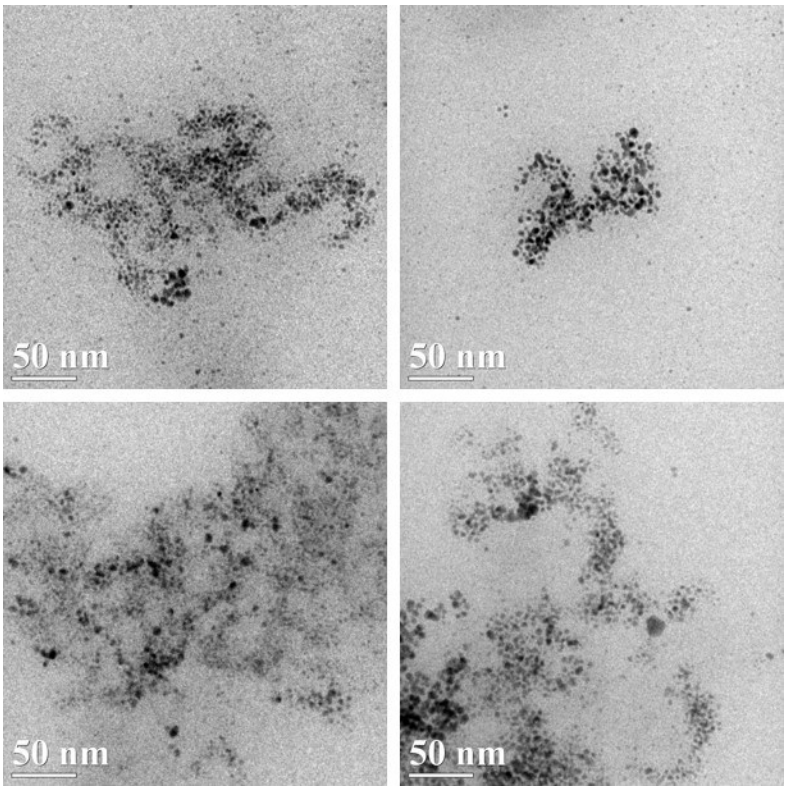

Figure S17. Additional TEM images of 1:1 (Ag, Au):*trans* PARE.

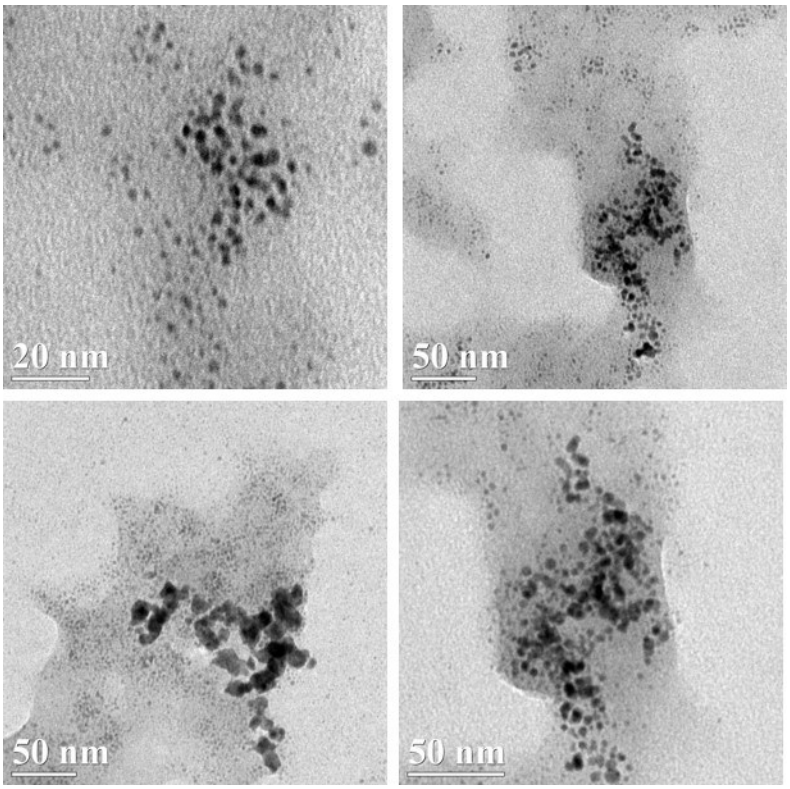

Figure S18. Additional TEM images of 2:1 (Ag, Au):*trans* PARE.

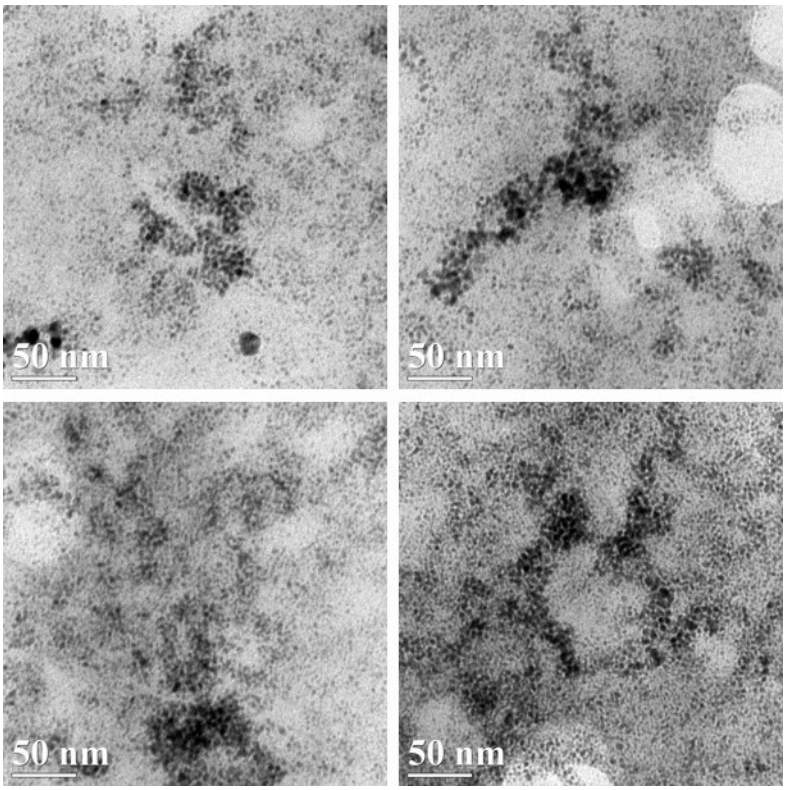

Figure S19. Additional TEM images of 3:1 (Ag, Au):*trans* PARE.

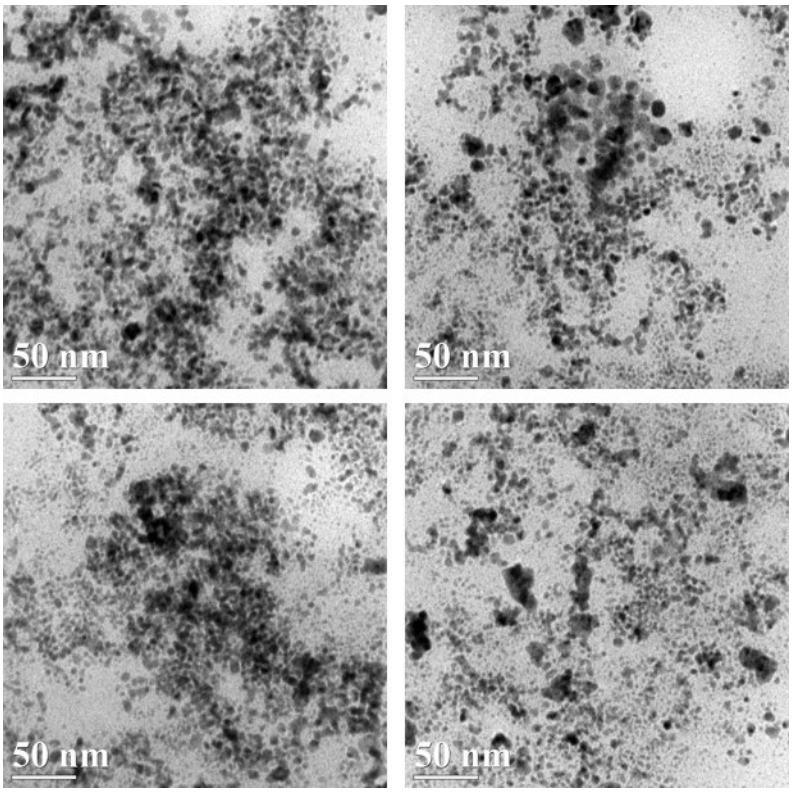

Figure S20. Additional TEM images of 4:1 (Ag, Au):*trans* PARE.

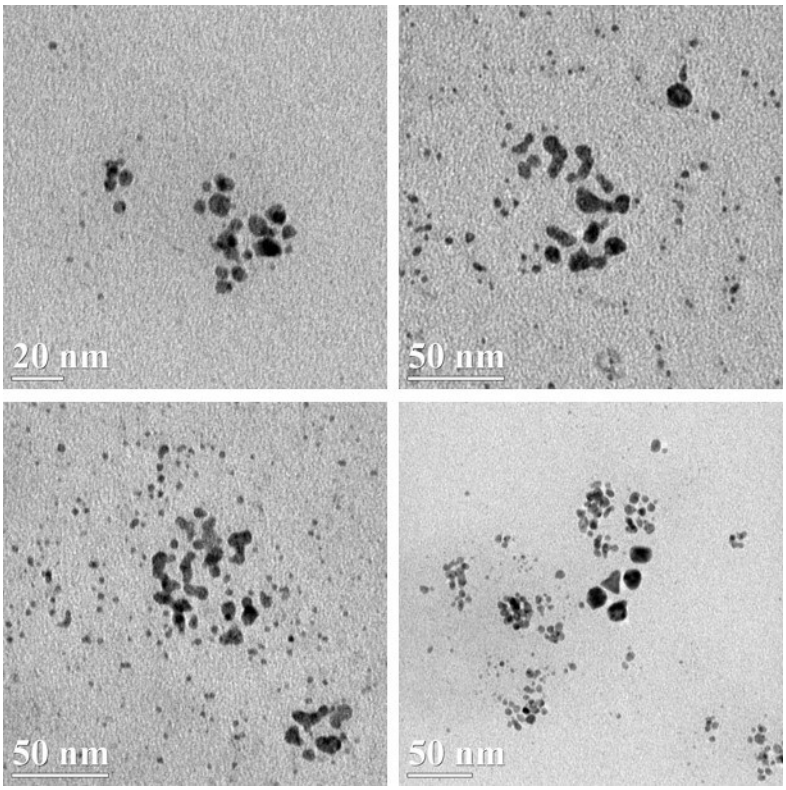

Figure S21. Additional TEM images of 1:1 (Ag, Au):*cis* PARE.

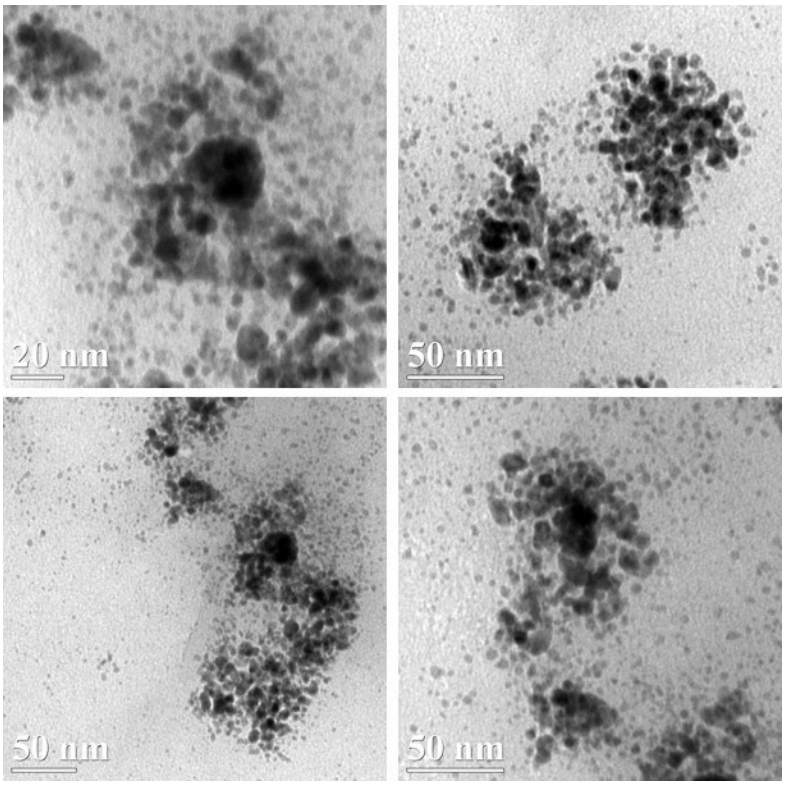

Figure S22. Additional TEM images of 2:1 (Ag, Au):*cis* PARE.

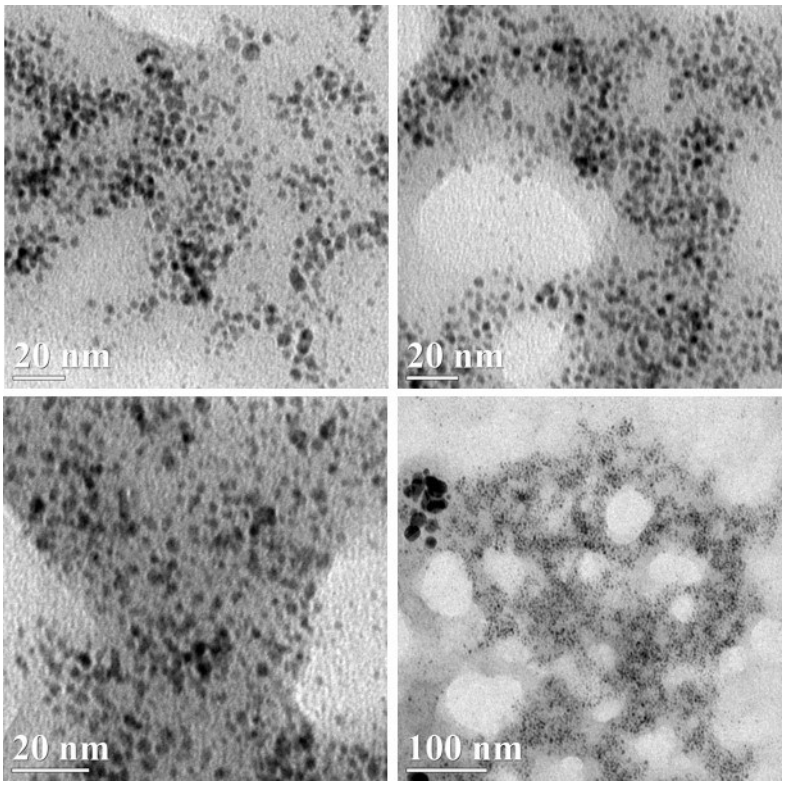

Figure S23. Additional TEM images of 3:1 (Ag, Au):*cis* PARE.

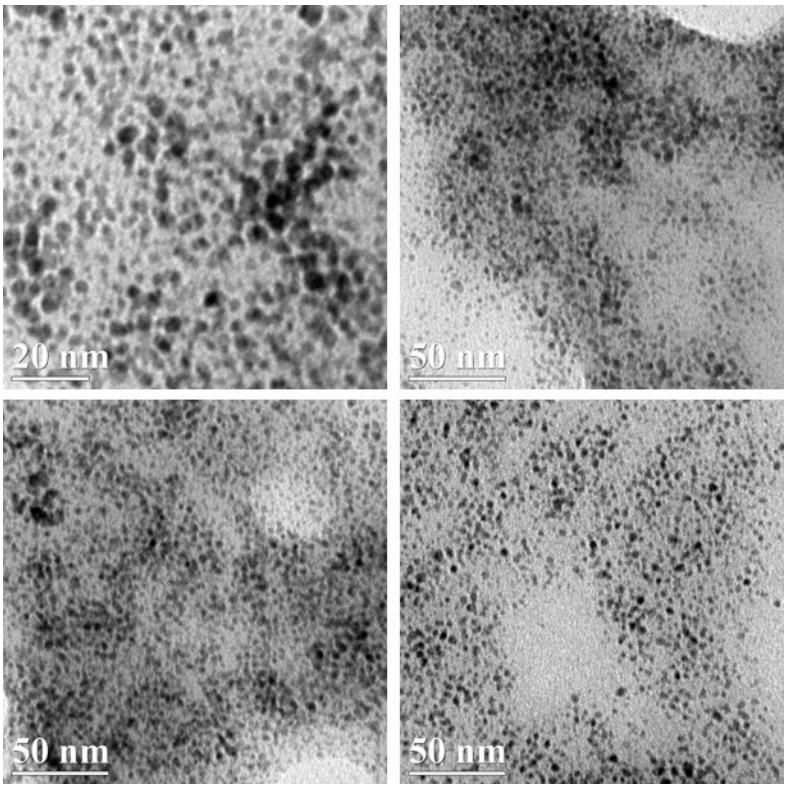

Figure S24. Additional TEM images of 4:1 (Ag, Au):*cis* PARE.

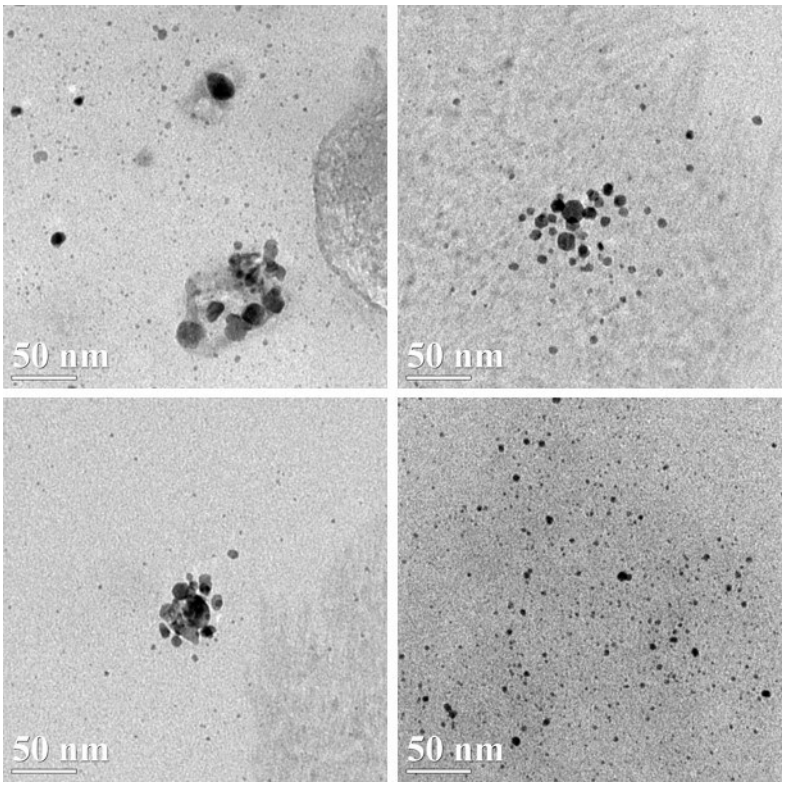

Figure S25. Additional TEM images of 1:1 (Au, Ag):*trans* PARE.

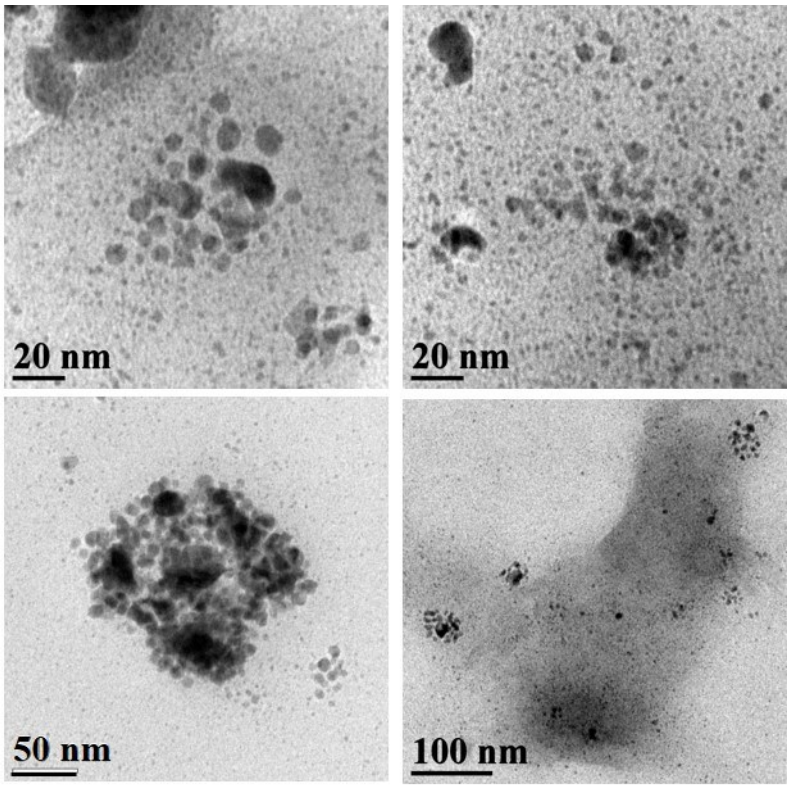

Figure S26. Additional TEM images of 2:1 (Au, Ag):*trans* PARE.

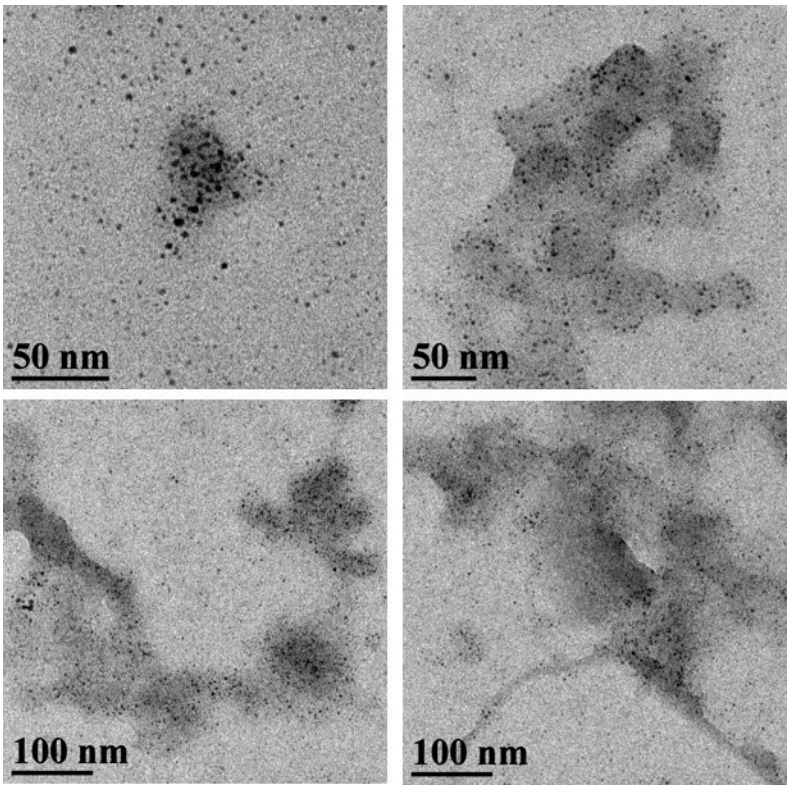

Figure S27. Additional TEM images of 3:1 (Au, Ag):*trans* PARE.

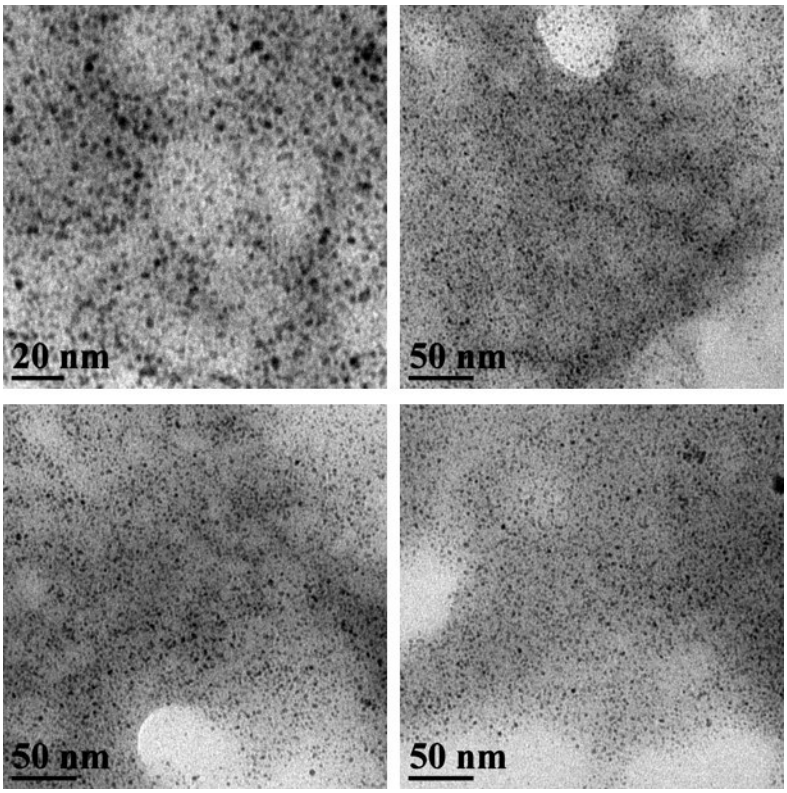

Figure S28. Additional TEM images of 4:1 (Au, Ag):*trans* PARE.

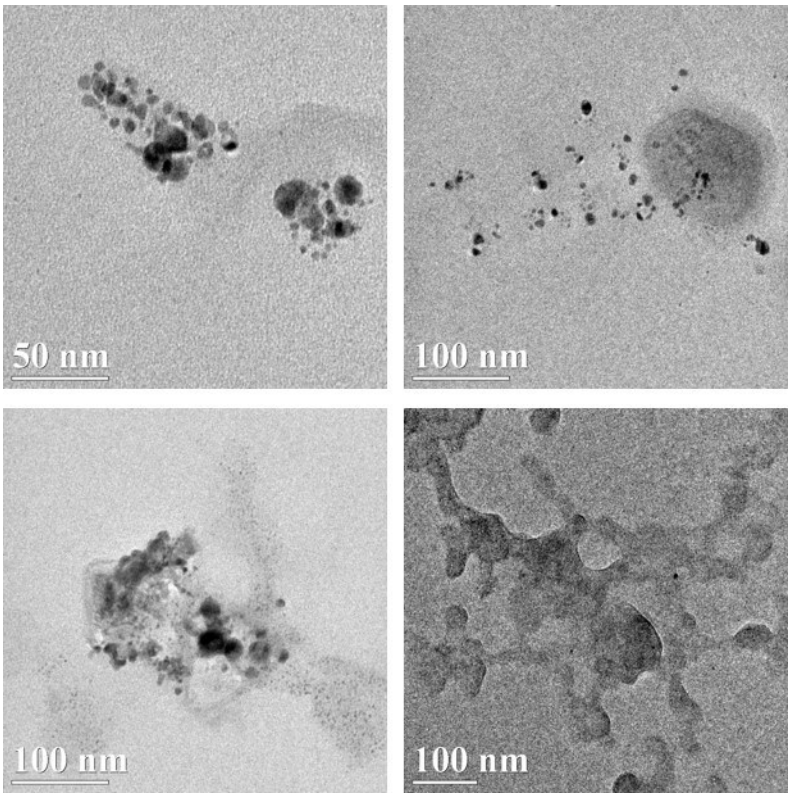

Figure 29. Additional TEM images of 1:1 (Au, Ag):*cis* PARE.

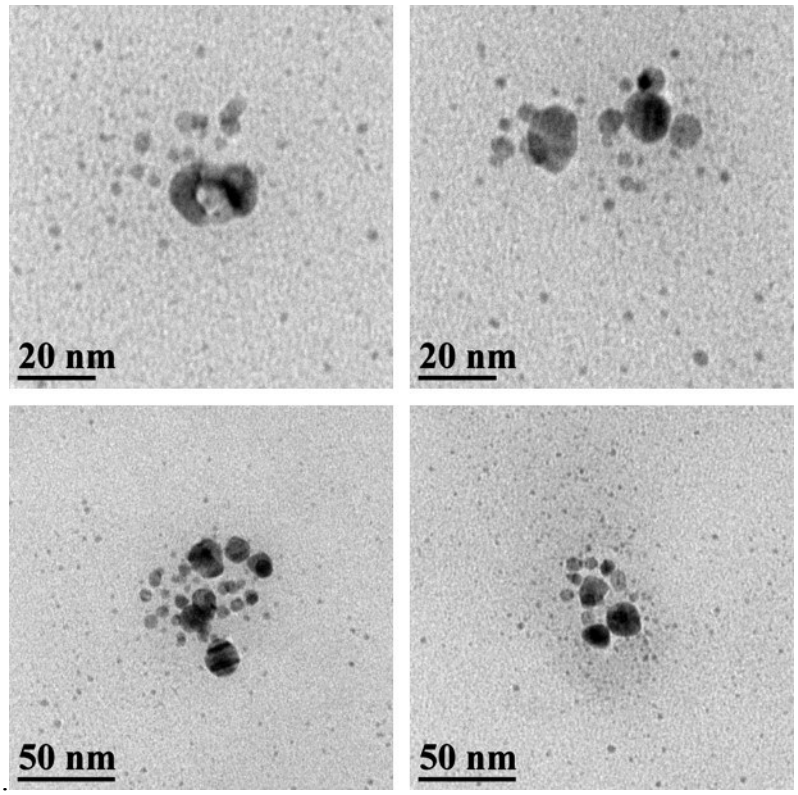

Figure 30. Additional TEM images of 2:1 (Au, Ag):*cis* PARE.

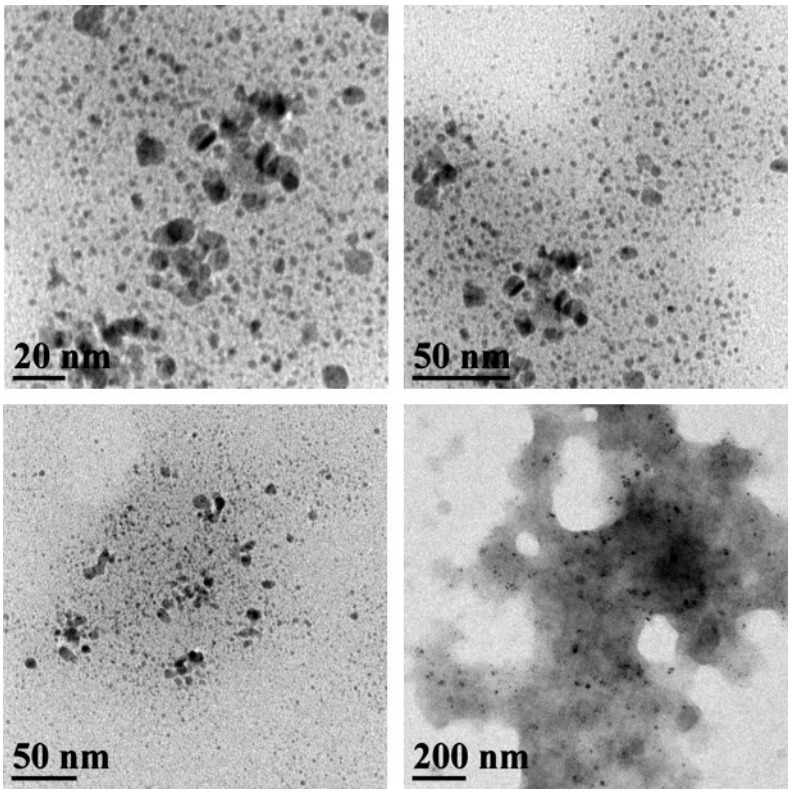

Figure 31. Additional TEM images of 3:1 (Au, Ag):*cis* PARE.

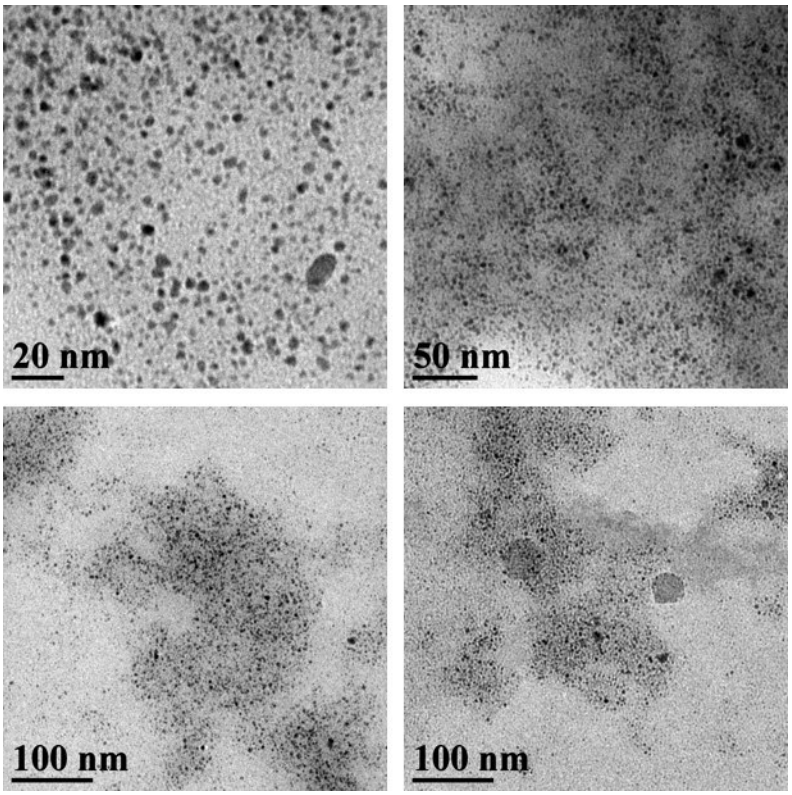

Figure 32. Additional TEM images of 4:1 (Au, Ag):*cis* PARE.

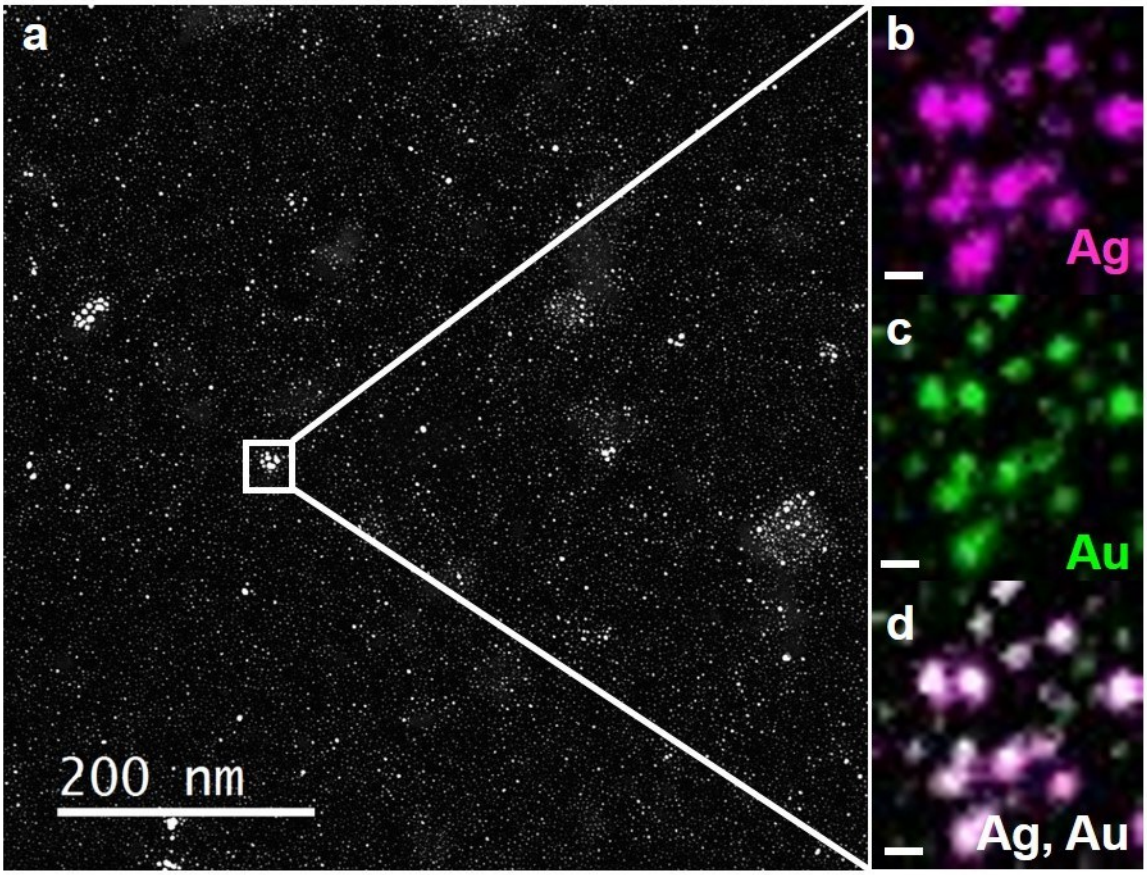

Figure S33. Dark-field TEM Image and EDS mapping of assemblies at a metal:PARE ratio of 2. Shown here is (Ag, Au):*trans* PARE. Inset scale on EDS mapping is 5 nm.

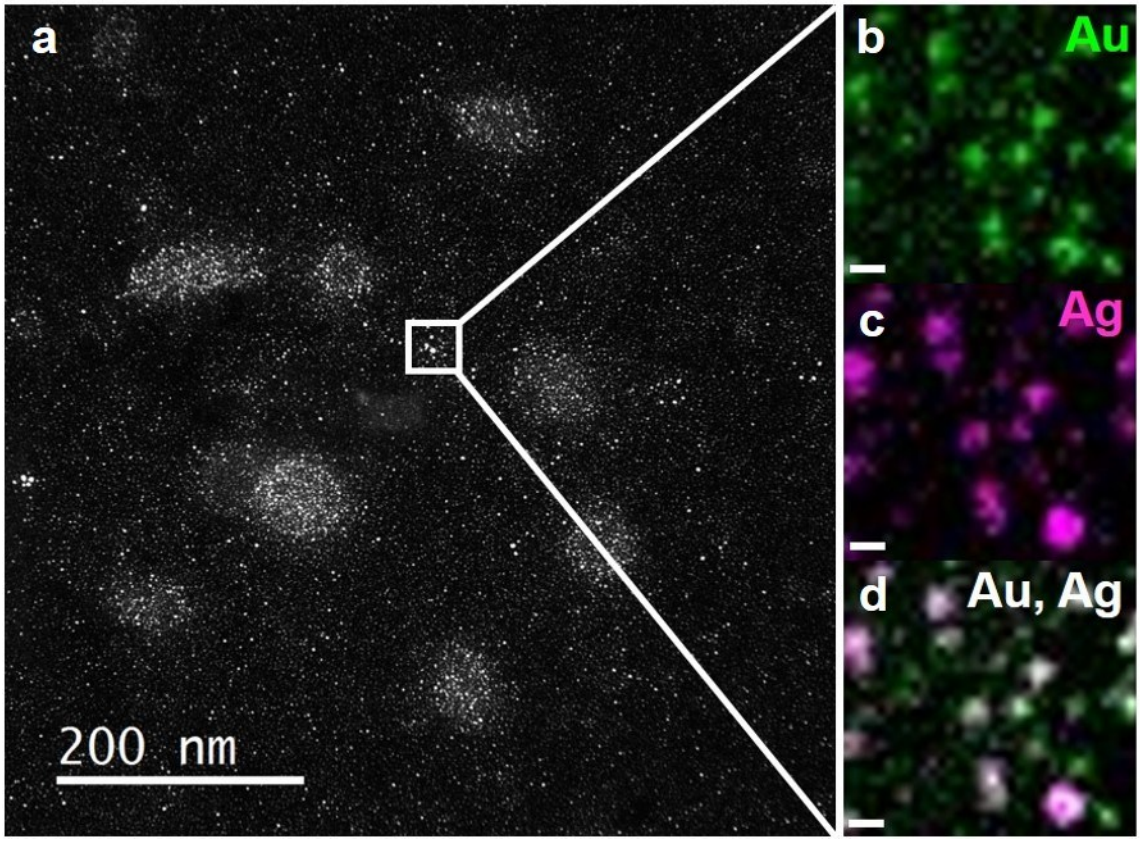

Figure S34. Dark-field TEM Image and EDS mapping of assemblies at a metal:PARE ratio of 2. Shown here is (Au, Ag):*trans* PARE. Inset scale on EDS mapping is 5 nm.

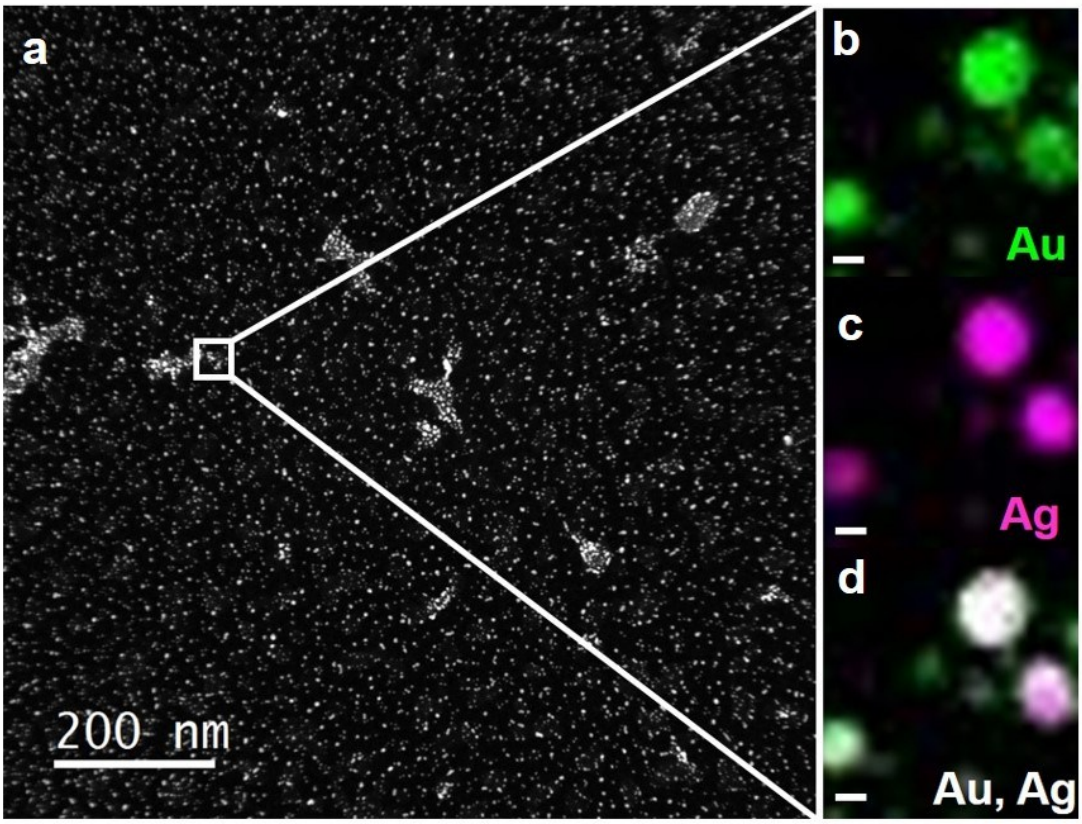

Figure S35. Dark-field TEM Image and EDS mapping of assemblies at a metal:PARE ratio of 2. Shown here is (Au, Ag):*cis* PARE. Inset scale on EDS mapping is 5 nm.

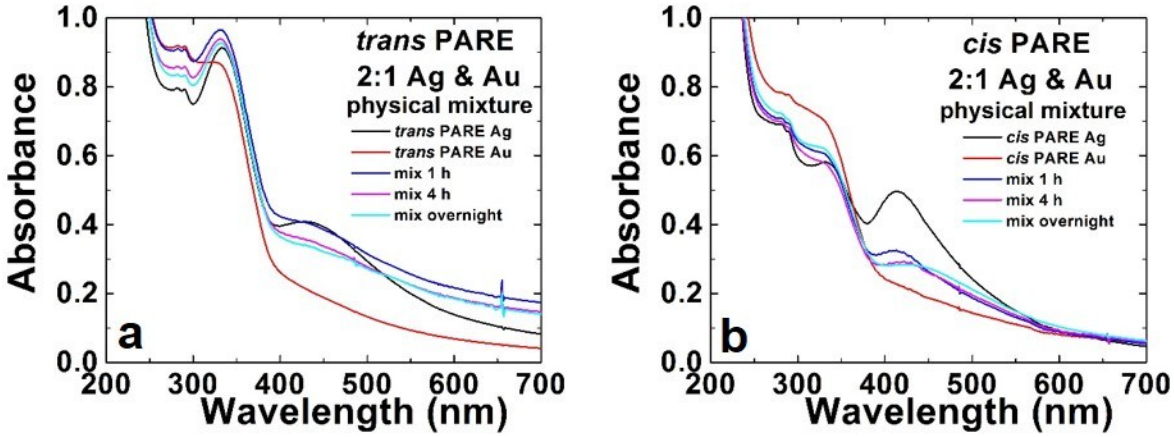

Figure S36. UV-vis spectra of physical mixture controls at metal:PARE ratio of 2. Part (a) shows the physical mixture of *trans* PARE Ag and *trans* PARE Au. Part (b) shows the physical mixture of *cis* PARE Ag and *cis* PARE Au.

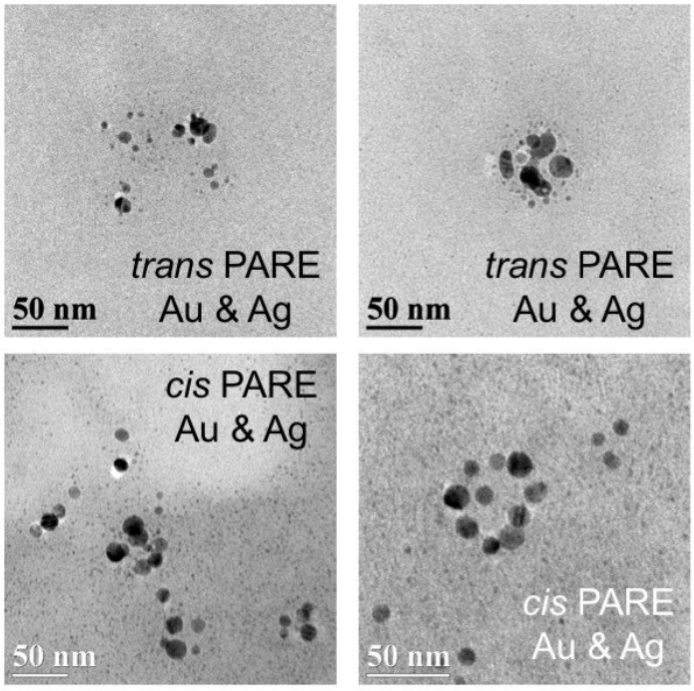

Figure S37. TEM images of physical mixture controls at a metal:PARE ratio of 2. The top row shows particles formed from the physical mixture of *trans* PARE Ag and *trans* PARE Au, while the bottom row shows particles formed from the physical mixture of *cis* PARE Ag and *cis* PARE Au.

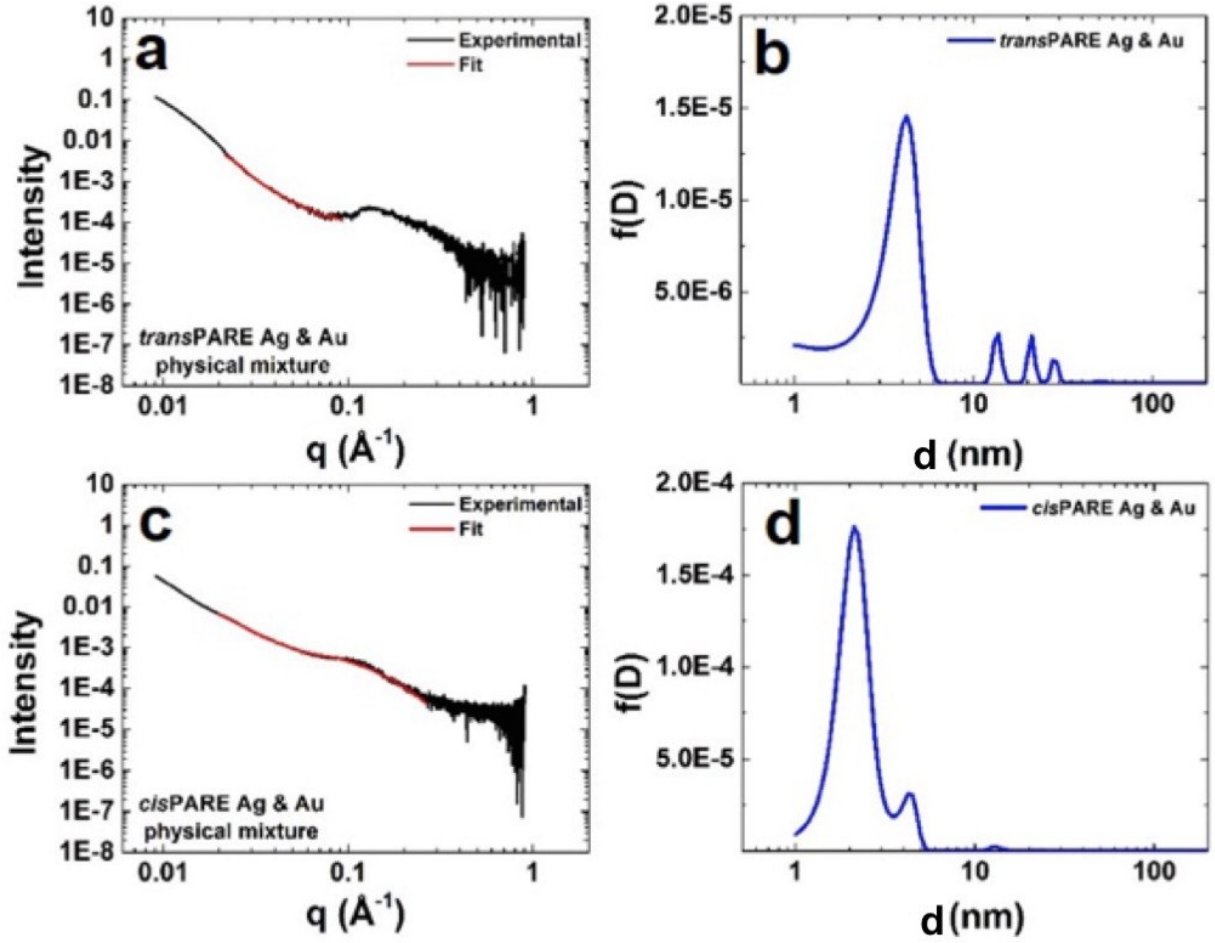

Figure S38. Physical mixtures SAXS spectra. All assemblies were prepared at a metal:PARE ratio of 2. Parts (a) and (c) show the scattering data and corresponding experimental fitting. Parts (b) and (d) show the size determined from the fitting.

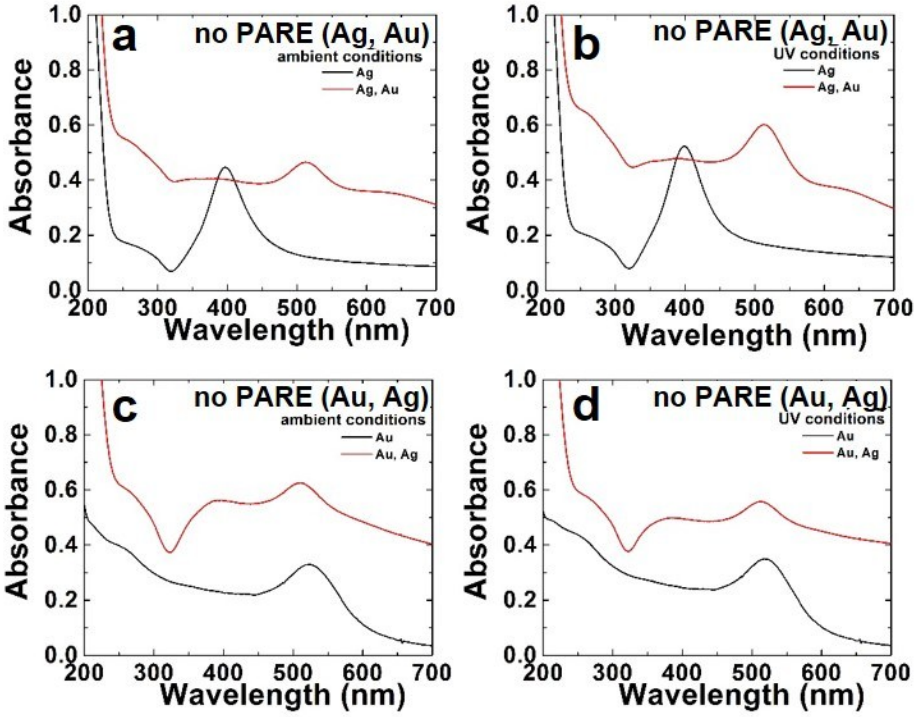

Figure S39. UV-vis spectra of no PARE control samples, prepared at the same concentration as the 2 ratio for the PARE samples. Part (a) corresponds to no PARE (Ag, Au) under ambient conditions while part (b) is the same under UV conditions. Part (c) shows no PARE (Au, Ag) under ambient conditions while part (d) is the same under UV conditions.

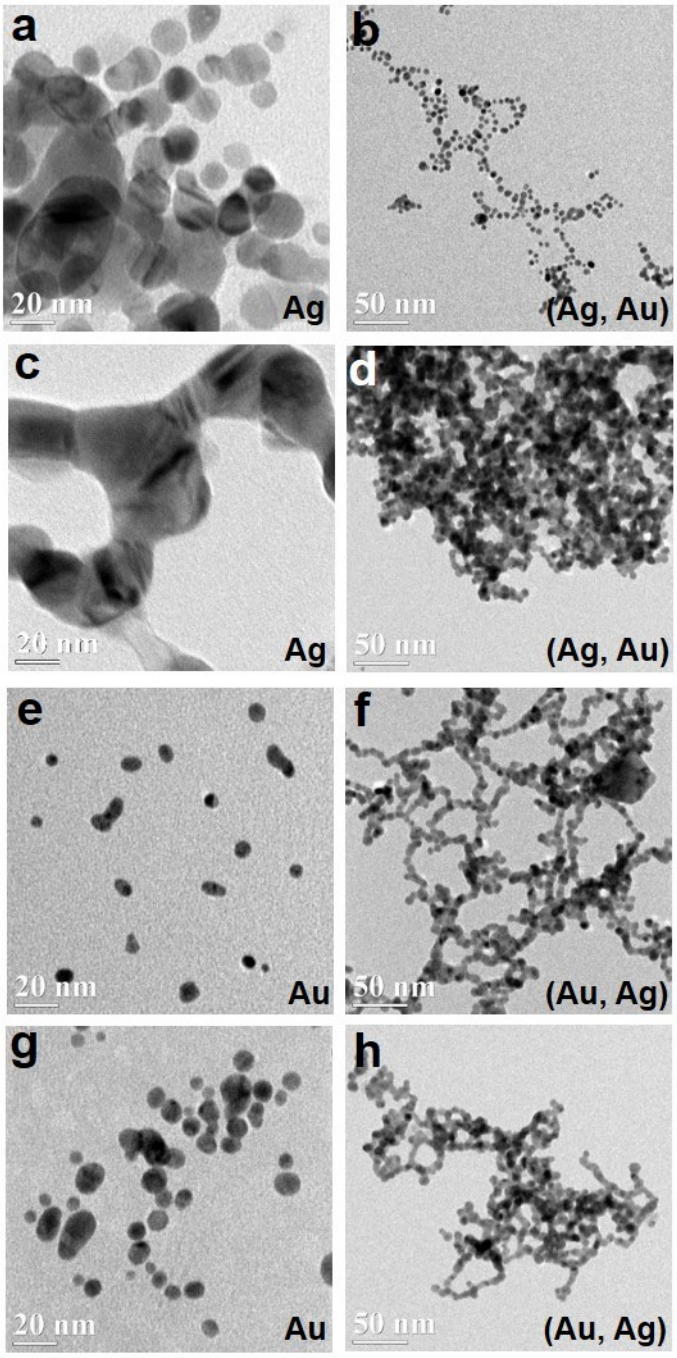

Figure S40. TEM of no PARE control samples. All samples were prepared at identical metal concentrations as the 2 ratio for the PARE assemblies. Part (a) is Ag under ambient conditions while (b) is (Ag, Au). Part (c) shows Ag under UV conditions while (d) is (Ag, Au). Part (e) is Au under ambient conditions while (f) is (Au, Ag). Part (g) shows Au under UV conditions while (h) is (Au, Ag).

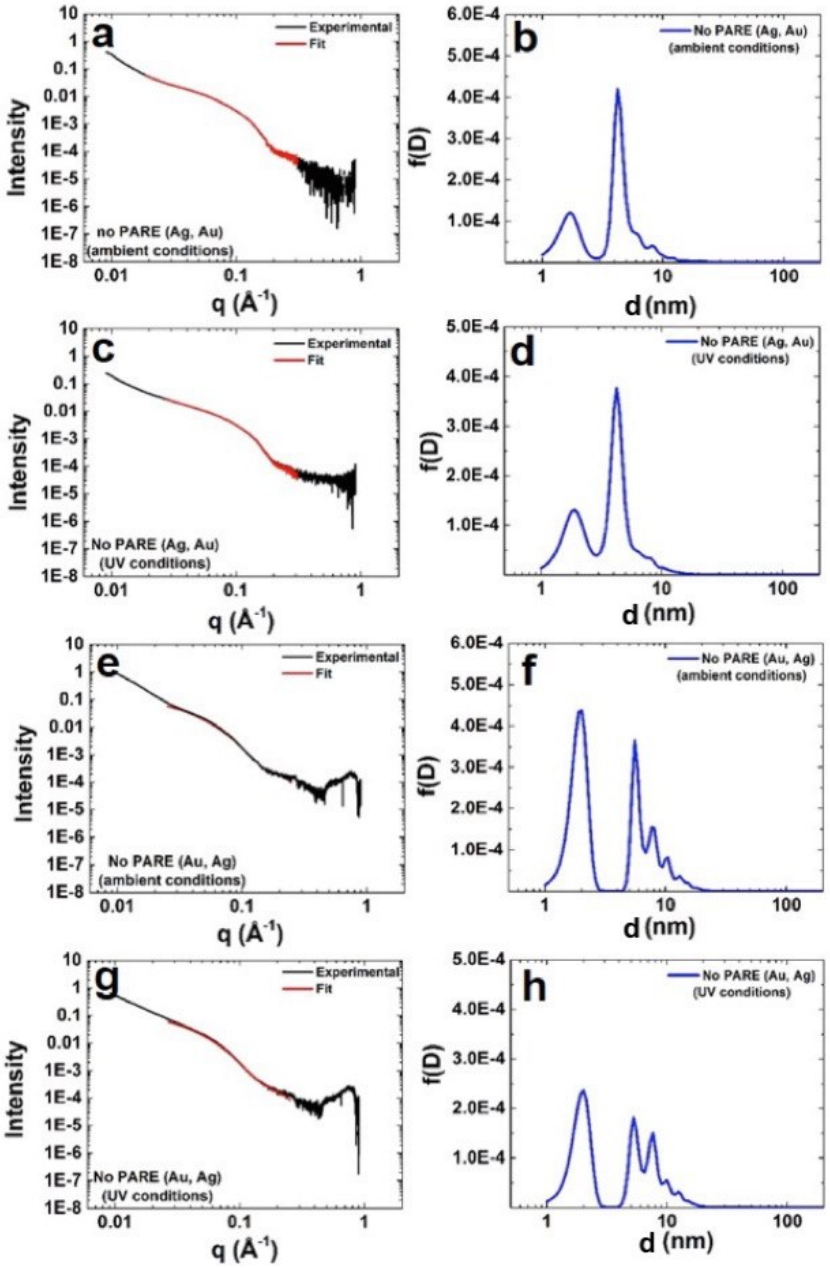

Figure S41. SAXS spectra for no PARE controls prepared at metal concentrations identical to the 2 ratio for the PARE samples. Parts (a, c, e and g) show the scattering with corresponding experimental fitting for no PARE controls while parts (b, d, f and h) are the extrapolated sizes from the fitting.

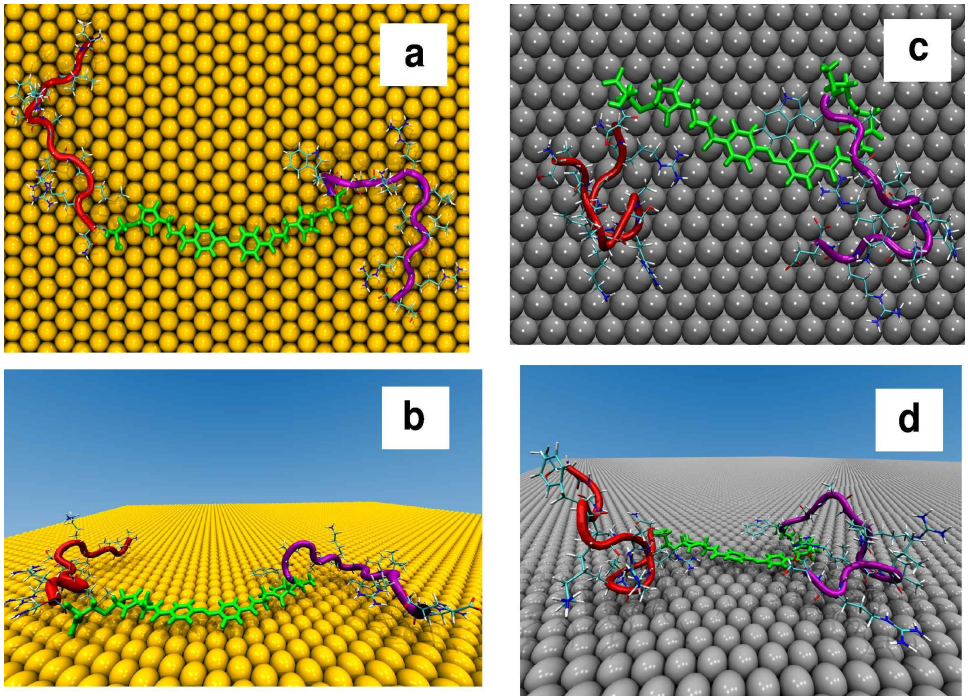

Figure S42. Most likely adsorbed conformations for the trans-PARE molecule, adsorbed at the aqueous Au(111) and Ag(111) interfaces, predicted from our REST simulations. a) plan view on Au, b) side view on Au, c) plan view on Ag, d) side view on Ag. Waters not shown for clarity. The AgBP1 backbone, AuBP1 backbone and MAM are highlighted in red, purple and green respectively.

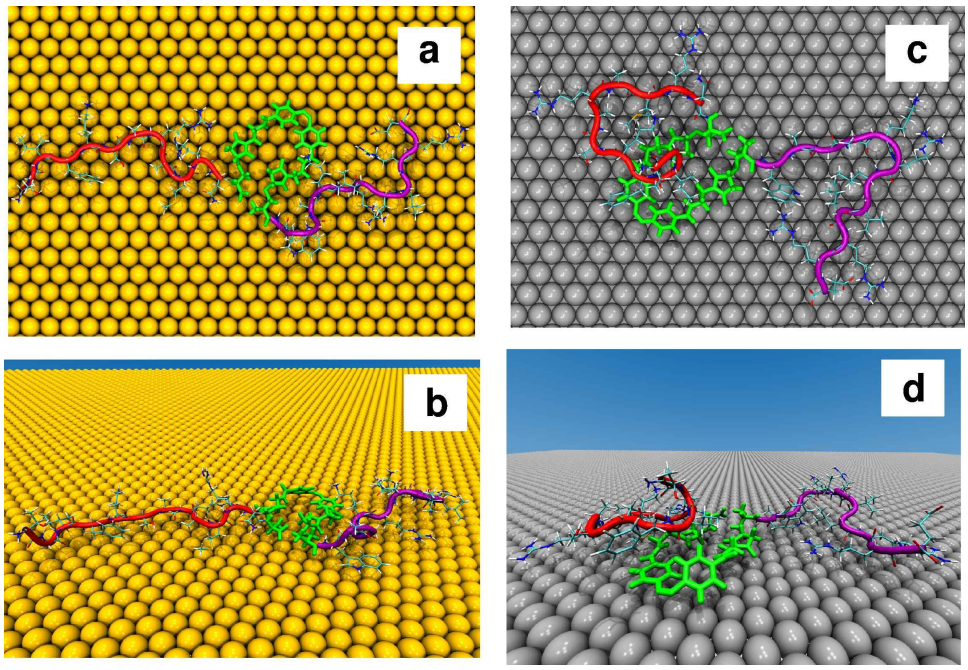

Figure S43. Most likely adsorbed conformations for the *cis*-PARE molecule, adsorbed at the aqueous Au(111) and Ag(111) interfaces, predicted from our REST simulations. a) plan view on Au, b) side view on Au, c) plan view on Ag, d) side view on Ag. Waters not shown for clarity. The AgBP1 backbone, AuBP1 backbone and MAM are highlighted in red, purple and green respectively.

Supporting Information: Computational Details

Replica-Exchange with Solute Tempering Simulations:

System Setup: Each system (4 systems in total) comprised one 5-layer Ag or Au slab presenting the (111) surface on both sides of the slab, one peptide chain, ~52260 water molecules, and, as required, six counter-ions (in the form of Cl^-) to ensure overall charge neutrality of the simulation cell. Each PARE was modelled with the zwitterionic form of the N- and C-termini of the peptides (*i.e*. no capping groups), consistent with the experimentally synthesized molecule, *e.g.* the N-terminus of the PARE (*i.e.* the N-terminus of AgBP1) was modelled as NH_3^+. Each residue in each hybrid molecule was assigned a protonation state consistent with a solution pH of ~7. We used an orthorhombic periodic cell; the metal slab had lateral dimensions approximately 123 Å x 122 Å, with an inter-slab spacing perpendicular to the slab surface in excess of 105 Å (such that the dimension of the cell perpendicular to the surface plane was ~ 116 Å). The dimension of the cell perpendicular to the surface plane was adjusted such that the density of liquid water in the central region between the slabs was consistent with the liquid water density at room temperature and ambient pressure. Periodic boundary conditions were applied in all three dimensions. All simulations were performed in the Canonical (*NVT*) ensemble, at a temperature of 300K, maintained using the Nosé-Hoover thermostat,[1] with a coupling constant of τ = 0.4 ps. Newton's equations of motion were solved using the leapfrog algorithm with an integration time-step of 1fs. Coordinates and velocities were saved every 1000 steps (1ps). Long-ranged electrostatic interactions were treated using Particle-mesh Ewald (PME),[2] with a cut-off at 11 Å, whereas a force-switched cut-off, starting at 9 Å and ending at 10 Å was used for Lennard-Jones non-bonded interactions.

The GolP-CHARMM[3] and AgP-CHARMM[4] force-fields were used to model the Au and Ag slabs respectively. The peptide was described using the CHARMM22*[5] force-field, and water was described using TIPS3P.[6] All metal atoms in the slab were held fixed in space during these simulations, with only the metal atom dipoles able to freely rotate. Random initial dipole positions were used throughout. Our recent tests indicate that there is very little difference between binding obtained using a rigid substrate, *vs*. using a slab where all atoms can move.[7] Details of the force-field modifications required to model the maleimide-azobenzene-maleimide (MAM) moiety were provided in a previous study.[8]

REST Details: Our implementation of REST exploits the replica exchange and free energy perturbation theory functionalities within Gromacs 4.5.5.[9] Details of the Terakawa implementation[10] of REST have been given by us previously.[11] In our REST simulations, we spanned an 'effective temperature' window of 300-500K with 16 replicas. The initial configurations for each replica cover a range of secondary structures, including α-helix, β-turn, polyproline II and random coil conformations for the peptide component of the PARE, and either the *trans* or the *cis* conformation for the MAM component of the molecule. The adsorbate structure for each replica was initially placed so that at least one peptide atom was within ~3Å distance from the top surface of either the Au slab or the Ag slab. The 16 values of lambda used to scale our force-field were:
λ_j = 0.0000, 0.057, 0.114, 0.177, 0.240, 0.310, 0.382, 0.458, 0.528, 0.597, 0.692, 0.750, 0.803, 0.855, 0.930, 1.0000.

Prior to each REST simulation, initial configurations were equilibrated at their target potential for 0.5 ns, with no exchange moves attempted during this time. The interval between exchange attempts set to 1000 MD steps (every 1 ps). All production REST simulations were run for a total of 50×10^6 MD steps (50 ns).

Evidence of the sampling efficacy of the REST approach is given in Figure S44, where our example shows the typical high degree of mobility of the replicas through lambda space.
In Figure S45, we show an example of evidence used to determine sample equilibration, namely the number of clusters vs. REST MD steps for the unscaled, reference replica ($\lambda = 0.000$).

REST MD clustering analysis: Detailed analysis was carried out on the constant-ensemble run at an effective temperature of 300K (herein referred to as the reference trajectory). We classified the Boltzmann-weighted ensemble from our reference trajectories into groups of like structures, on the basis of similarity of their backbone structures, *via* the Daura clustering algorithm[12] with a root mean-squared deviation (RMSD) cutoff between the positions all peptide backbone atoms. We used two definitions of the backbone; in the first, the backbone was denoted by both of the peptide backbone atoms plus the atoms along the mid-line of the MAM unit (we denote this as clustering over the entire molecule); in the second, we considered only the backbone of the AuBP1 and AgBP1 sequences within the PARE, to enable direct comparison with our previously published data on the parent peptide. In the former case, the RMSD cutoff was 5 Å, in the latter we used a cutoff of 2 Å. In general, RMSD cutoffs used in clustering analyses are size-extensive, such that the cutoff should be adjusted to be commensurate with the size of the molecule. The cutoff of 2 Å was identified via extensive testing conducted on dodecapeptides[11] from which we found a cutoff of 2 Å to yield an appropriately sensible balance between resolution and meaningful structural similarity. The PARE molecule is larger and therefore it is appropriate to use a larger cutoff in this case. Again, our extensive testing identified a cutoff of 4Å to be reasonable in this instance. We emphasize here that it is not appropriate to directly compare clustering data obtained with different cutoffs. We performed our clustering analysis over the entire 50 ns trajectory in each case. The population of a given cluster was calculated as the percentage fraction of the number of frames that were assigned membership of that cluster, divided by the total number of frames in the trajectory. The cluster with the largest population corresponds with the most likely structure of the PARE in the interface-adsorbed state.

REST MD Contact Residue analysis: We define a contact residue as a residue that maintains strong contact with the surface. To quantify this contact, first, for each reference trajectory, we calculated the distance between the topmost layer of the Au/Ag surface and each residue in the AuBP1/AgBP1 sequences, and each of the five sites in the MAM (the two maleimide rings, two phenyl rings and the central N=N bond). On the basis of these data, distance cut-offs were established to identify a range of separations where each particular residue, including the MAM unit, was in immediate contact with the Au/Ag surface. We then calculated the fraction of frames in the reference trajectory for which each residue was found within the contact range of surface-residue separation. We then defined a residue to be a contact residue if that residue was found to bind persistently to the surface. Our definition of persistent contact was satisfied if the given residue was found within contact range for 60% of more of the last 5 ns of the reference trajectory. Further details including the data used to establish the cutoffs, and further analysis

based on variation of both the contact cutoff distance and the percentage of frames required to satisfy our definition of a contact residue can be found in our previous work.[8, 13]

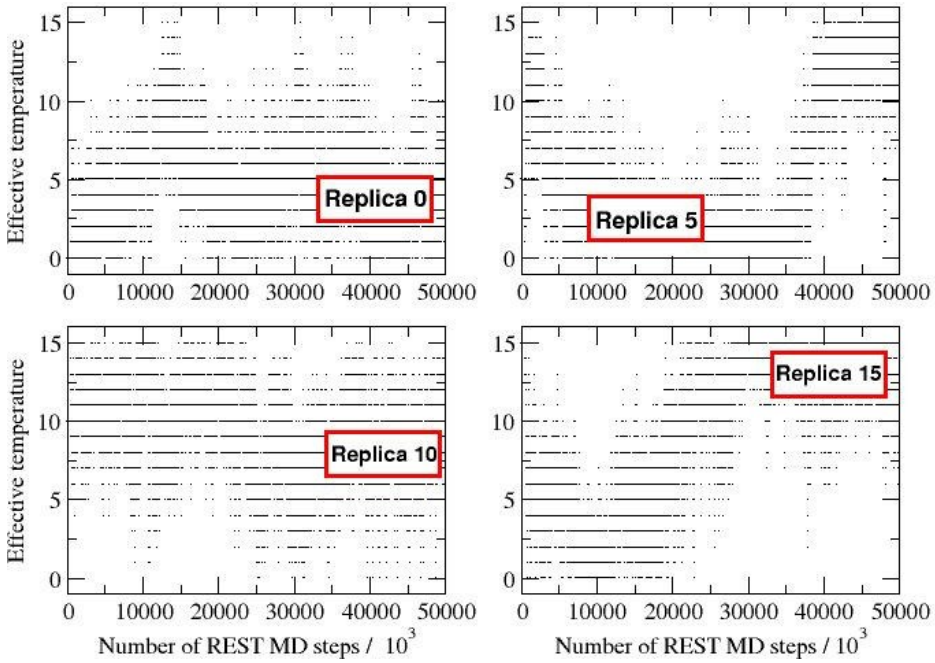

Figure S44. Exemplar effective temperature mobilities for 4 out of the 16 replicas, for the *trans*-PARE REST simulation adsorbed at the aqueous Au(111) interface.

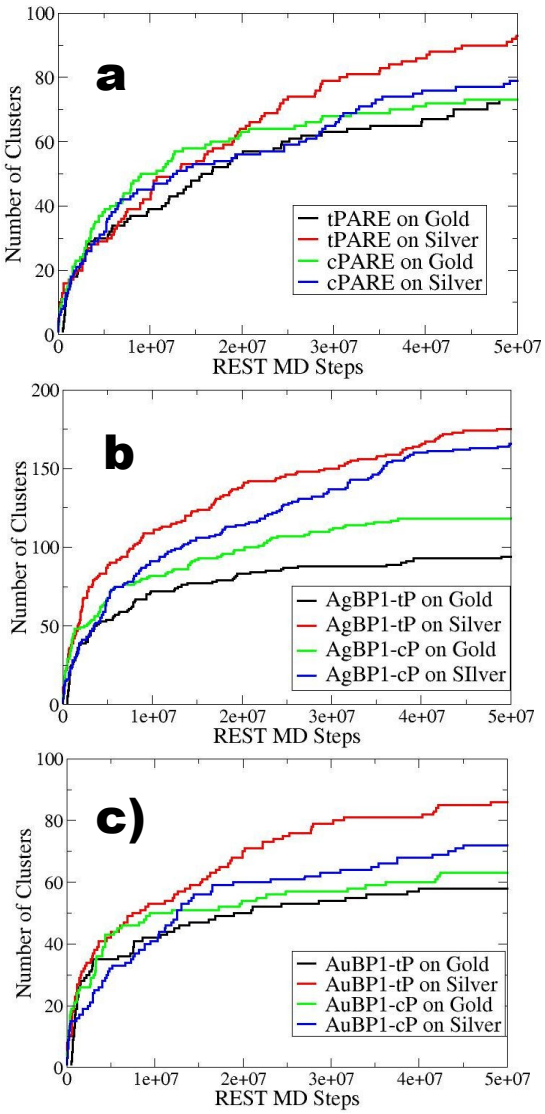

Figure S45. Number of clusters as a function of MD steps, shown for the reference REST trajectory, determined for adsorption at the aqueous Au(111) and Ag(111) interfaces for **a)** the entire PARE molecule (clustering cut-off of 5 Å), **b)** the AgBP1 component of the PARE molecule (clustering cut-off of 2 Å), and **c)** the AuBP1 component of the PARE molecule (clustering cut-off of 2 Å). The labels "t" and "c" denote *trans* and *cis* isomerization states of the MAM unit in the PARE molecule.

1. (a) Nose, S., A Molecular-Dynamics Method for Simulations in the Canonical Ensemble. *Mol Phys* **1984,** *52* (2), 255-268; (b) Hoover, W. G., Canonical dynamics: Equilibrium phase-space distributions. *Physical Review A* **1985,** *31*, 1695 - 1697.
2. Darden, T.; York, D.; Pedersen, L., Particle Mesh Ewald - an N.Log(N) Method for Ewald Sums in Large Systems. *J Chem Phys* **1993,** *98* (12), 10089-10092.
3. (a) Wright, L. B.; Rodger, P. M.; Corni, S.; Walsh, T. R., GoIP-CHARMM: First-Principles Based Force Fields for the Interaction of Proteins with Au(111) and Au(100). *J Chem Theory Comput* **2013,** *9* (3), 1616-1630; (b) Wright, L. B.; Rodger, P. M.; Walsh, T. R.; Corni, S., First-Principles-Based Force Field for the Interaction of Proteins with Au(100)(5 x 1): An Extension of GoIP-CHARMM. *J Phys Chem C* **2013,** *117* (46), 24292-24306.
4. Hughes, Z. E.; Wright, L. B.; Walsh, T. R., Biomolecular Adsorption at Aqueous Silver Interfaces: First-Principles Calculations, Polarizable Force-Field Simulations, and Comparisons with Gold. *Langmuir* **2013,** *29* (43), 13217-13229.
5. (a) MacKerell, A. D.; Bashford, D.; Bellott, M.; Dunbrack, R. L.; Evanseck, J. D.; Field, M. J.; Fischer, S.; Gao, J.; Guo, H.; Ha, S.; Joseph-McCarthy, D.; Kuchnir, L.; Kuczera, K.; Lau, F. T. K.; Mattos, C.; Michnick, S.; Ngo, T.; Nguyen, D. T.; Prodhom, B.; Reiher, W. E.; Roux, B.; Schlenkrich, M.; Smith, J. C.; Stote, R.; Straub, J.; Watanabe, M.; Wiorkiewicz-Kuczera, J.; Yin, D.; Karplus, M., All-atom empirical potential for molecular modeling and dynamics studies of proteins. *J Phys Chem B* **1998,** *102* (18), 3586-3616; (b) Piana, S.; Lindorff-Larsen, K.; Shaw, D. E., How Robust Are Protein Folding Simulations with Respect to Force Field Parameterization? *Biophys J* **2011,** *100* (9), L47-L49.
6. (a) Jorgensen, W. L.; Chandrasekhar, J.; Madura, J. D.; Impey, R. W.; Klein, M. L., Comparison of Simple Potential Functions for Simulating Liquid Water. *J Chem Phys* **1983,** *79* (2), 926-935; (b) Neria, E.; Fischer, S.; Karplus, M., Simulation of activation free energies in molecular systems. *J Chem Phys* **1996,** *105* (5), 1902-1921.
7. Wright, L. B.; Freeman, C. L.; Walsh, T. R., Benzene adsorption at the aqueous (011) alpha-quartz interface: is surface flexibility important? *Mol Simulat* **2013,** *39* (13), 1093-1102.
8. Tang, Z. H.; Lim, C.-K.; Palafox-Hernandez, J. P.; Drew, K. L. M.; Li, Y.; Swihart, M. T.; Prasad, P. N.; Walsh, T. R.; Knecht, M. R., Triggering Nanoparticle Surface Ligand Rearrangement via External Stimuli: Light-based Actuation of Biointerfaces. *Nanoscale* **2015,** *DOI: 10.1039/C5NR02311D*.
9. Hess, B.; Kutzner, C.; van der Spoel, D.; Lindahl, E., GROMACS 4: Algorithms for highly efficient, load-balanced, and scalable molecular simulation. *J Chem Theory Comput* **2008,** *4* (3), 435-447.
10. Terakawa, T.; Kameda, T.; Takada, S., On Easy Implementation of a Variant of the Replica Exchange with Solute Tempering in GROMACS. *J Comput Chem* **2011,** *32* (7), 1228-1234.
11. Wright, L. B.; Walsh, T. R., Efficient conformational sampling of peptides adsorbed onto inorganic surfaces: insights from a quartz binding peptide. *Phys Chem Chem Phys* **2013,** *15* (13), 4715-4726.
12. Daura, X.; Gademann, K.; Jaun, B.; Seebach, D.; van Gunsteren, W. F.; Mark, A. E., Peptide folding: When simulation meets experiment. *Angew Chem Int Edit* **1999,** *38* (1-2), 236-240.
13. Palafox-Hernandez, J. P.; Tang, Z. H.; Hughes, Z. E.; Li, Y.; Swihart, M. T.; Prasad, P. N.; Walsh, T. R.; Knecht, M. R., Comparative Study of Materials-Binding Peptide Interactions with Gold and Silver Surfaces and Nanostructures: A Thermodynamic Basis for Biological Selectivity of Inorganic Materials. *Chem Mater* **2014,** *26* (17), 4960-4969.